Cell-based screen for altered nuclear phenotypes reveals senescence progression in polyploid cells after Aurora kinase B inhibition

Mahito Sadaie[*,¶], Christian Dillon[†], Masako Narita[*], Andrew R. J. Young[*], Claire J. Cairney[‡], Lauren S. Godwin[§], Christopher J. Torrance[||], Dorothy C. Bennett[§], W. Nicol Keith[‡], and Masashi Narita[*,#]

[*]Cancer Research UK Cambridge Institute, University of Cambridge, Li Ka Shing Centre, Robinson Way, Cambridge CB2 0RE, UK

[†]Cancer Research Technology Discovery Laboratories, Wolfson Institute for Biomedical Research, The Cruciform Building, Gower Street, London WC1E 6BT, UK

[‡]Institute of Cancer Sciences, Wolfson Wohl Cancer Research Centre, University of Glasgow, Garscube Estate, Switchback Road, Bearsden, Glasgow G61 1QH, UK

[§]St. George's, University of London, Cranmer Terrace, London SW17 0RE, UK

[||]Horizon Discovery Ltd, IQ Cambridge, Waterbeach Cambridge CB25 9TL, UK

[¶]Present address: Graduate School of Biostudies, Kyoto University, Kyoto 606-8501, Japan

[#]Correspondence: Masashi.Narita@cruk.cam.ac.uk

Running head: Senescence progression after abortive mitosis

Abbreviations used: AURK, aurora kinase; SAC, spindle assembly checkpoint; HDF, human diploid fibroblasts; TIS, therapy-induced senescence; SA-β-gal, senescence-associated beta-galactosidase; SAHF, senescence-associated heterochromatic foci; RIS, RAS-induced senescence; DMSO, dimethyl sulfoxide; IRG, hit compounds that induced an irregular nuclear shape; SPT, hit compounds that induced spotty morphologies; BrdU, 5-bromo-2'-deoxyuridine; DAPI, 4',6-diamidino-2-phenylindole

ABSTRACT

Cellular senescence is a widespread stress response and is widely considered to be an alternative cancer therapeutic goal. Unlike apoptosis, senescence is composed of a diverse set of sub-phenotypes; depending on which of its associated effector programs are engaged. Here we establish a simple and sensitive, cell-based, pro-senescence screen with detailed validation assays. We have characterized the screen using a focused tool compound kinase inhibitor library. We have identified a series of compounds that induce different types of senescence, including a unique phenotype associated with irregularly shaped nuclei and the progressive accumulation of pseudo-G1 tetraploidy in human diploid fibroblasts. Downstream analyses showed that all those compounds that induced tetraploid senescence, inhibited Aurora kinase B (AURKB). AURKB is the catalytic component of the chromosome passenger complex, which is involved in correct chromosome alignment and segregation, the spindle assembly checkpoint (SAC), and cytokinesis. Although aberrant mitosis and senescence have been linked, a specific characterization of AURKB in the context of senescence is still required. This proof-of-principle study suggests that our protocol is capable of amplifying tetraploid senescence, which can be observed only in a small population of oncogenic RAS-induced senescence, and provides additional justification for AURKB as a cancer therapeutic target.

INTRODUCTION

Cellular senescence is a state of stable or 'irreversible' cell cycle arrest induced by various cytotoxic factors, including telomere dysfunction, DNA damage, oxidative stress, oncogenic stress, and some type of cytokines (Correia-Melo *et al.*, 2014; Salama *et al.*, 2014) Although senescence was originally defined in normal human diploid fibroblasts (HDFs), the best-characterized culture model of senescence, a similar phenotype can be induced in a wide range of cell types as well as in *in vivo* contexts that are associated with various pathophysiological contexts, such as tumorigenesis (Pérez-Mancera *et al.*, 2014), tissue repair (Krizhanovsky *et al.*, 2008; Jun and Lau, 2010), ageing (López-Otín *et al.*, 2013), and more recently embryogenesis (Chuprin *et al.*, 2013; Muñoz-Espín *et al.*, 2013; Storer *et al.*, 2013). Among all these, oncogene-induced senescence (OIS), where excessive mitogenic stress provokes senescence effectors leading to progressive development of senescence phenotypes in culture and animal models, underscores the tumour suppressor role of senescence. In addition, it has been shown that senescence can also be induced by chemotherapeutic reagents in tumours (therapy-induced senescence, TIS), particularly in apoptosis-defective contexts (Poele *et al.*, 2002; Schmitt *et al.*, 2002; Xue *et al.*, 2007; Gewirtz *et al.*, 2008; Ewald *et al.*, 2010; Dörr *et al.*, 2013). Therefore, senescence has been considered as not only an intrinsic tumour suppressor but also an alternative therapeutic goal in cancer (Acosta and Gil, 2012; Cairney *et al.*, 2012). However, it has been shown that senescence may also facilitate tumorigenesis: senescent cells often secrete a wide range of soluble factors, which confer a considerable impact on the tumour microenvironment and local immune response, providing anti- and/or pro-tumorigenic effects depending on the context (Coppé *et al.*, 2010; Pérez-Mancera *et al.*, 2014).

Senescence is typically a dynamic and a long-term process, which can involve many regulatory effector mechanisms, conferring a diverse and heterogeneous nature to the phenotype (Salama *et al.*, 2014). Thus to qualitatively evaluate the senescence phenotype, various cellular and biochemical markers have been identified. Senescence markers include accumulation of senescence-associated-β-galactosidase (SA-β-gal) activity, a persistent DNA damage response, the senescence-associated secretory phenotype (SASP) (Kuilman and Peeper, 2009; Coppé *et al.*, 2010), and autophagy (Salama *et al.*, 2014). In addition, senescence is typically accompanied by enlarged cellular morphology with increased vesicular formation. Nuclei also can show distinct morphologic changes, including an enlargement of the nuclei and the nucleoli (Mitsui and Schneider, 1976; Bemiller and Lee, 1978), formation of senescence-associated heterochromatic foci (SAHF) (Narita *et al.*, 2003; Zhang *et al.*, 2005), up-regulation of promyelocytic leukemia (PML) nuclear bodies both in size and number (Ferbeyre *et al.*, 2000; Pearson *et al.*, 2000; Bischof *et al.*, 2002; 2005), alterations of lamin B1 and other components of the nuclear envelope (Maeshima *et al.*, 2006; Barascu *et al.*, 2012; Freund *et al.*, 2012; Dreesen *et al.*, 2013; Sadaie *et al.*, 2013; Shah *et al.*, 2013), and alteration of nuclear shape (Matsumura *et al.*, 1979) (reviewed in (Goldstein, 1990; Cristofalo and Pignolo, 1993)). Hence it has been proposed that it is necessary to combine multiple markers, which can be either more common to or unique to different contexts, along with the validation of stable exit from the cell cycle, required for the phenotype to qualify as senescence (Campisi, 2013; Salama *et al.*, 2014).

AURKB is a member of the aurora family, which also comprises related kinases, AURKA and AURKC. Both AURKA and AURKB are ubiquitously expressed but their subcellular localization, binding partners, and substrates are highly distinctive. The different isoforms are thus involved in different aspects of cell cycle regulation, whereas AURKC is mainly expressed in testis and its function is not well-characterized (Gautschi *et al.*, 2008). While AURKA is a centrosomal protein, mainly related to centrosome function and bipolar spindle assembly, AURKB, the catalytic component of the chromosome passenger complex, plays a key role in correct chromosomal alignment and segregation by destabilising erroneous kinetochore-microtubule attachments, and is thought to be involved in the spindle assembly checkpoint (SAC). It also has a critical role in cytokinesis (Kelly and Funabiki, 2009; Lens *et al.*, 2010; Carmena *et al.*, 2012). Inhibition of AURKB in cell culture leads to a failure to bi-orientate chromosomes, perturbed cytokinesis and as a consequence, causes polyploidization and an eventual loss of viability (Ditchfield *et al.*, 2003; Kaestner *et al.*, 2009; Lens *et al.*, 2010). It was recently shown that AURKs inhibitors that are more selective for AURKA induce senescence in melanoma cells (Liu *et al.*, 2013). On the other hand, it has also previously been shown that the ectopic expression of AURKB in normal HDFs induces senescence (Jung *et al.*, 2005). A more recent study, however, reported that AURKB overexpression delays senescence and siRNA-mediated AURKB knockdown induces senescence in HDFs (Kim *et al.*, 2011). Thus there is room for a more detailed characterization of the senescence phenotype caused by the modulation of AURKB expression, and more specifically, enzymatic activity.

Due to the diverse nature of senescence, identifying or developing senescence inducing factors would not only extend our cancer therapeutic modalities, it would also help in elucidating the effector mechanisms of senescence. While numerous genetic ‘senescence bypass’ screens have been successfully conducted (Jacobs *et al.*, 2000; Shvarts *et al.*, 2002; Gil *et al.*, 2004; Acosta *et al.*, 2008; Kortlever *et al.*, 2008; Leal *et* *al.*, 2008; Rovillain *et al.*, 2011), attempts at 'senescence inducing' screens are still limited (Ewald *et al.*, 2009; Lahtela *et al.*, 2013). Here, taking advantage of a high content fluorescence image analyzing system, we set out simple primary screens for small molecules that can induce senescence-related nuclear phenotypes, namely an enlargement in nuclear size and SAHF-like chromatin spottiness, in HDFs, followed by secondary analyses for detailed senescence validation in both HDFs and tumour cell lines. Using a kinase inhibitor library, we identified compounds that induce senescence with different nuclear morphologies. Interestingly, although the substrate specificities of the kinase inhibitors used were rather limited, a subset of the hit compounds converged on AURKB to induce a unique senescence phenotype, where pseudo-G1 tetraploidy or polyploidy progressively accumulated. Our study provides a simple and sensitive pro-senescence screen and the data reinforce the relevance of AURKB as a cancer therapeutic target.

RESULTS

Identification of small-molecule compounds that induce senescence-associated morphological changes in nuclei

To establish an image-based screen for senescence inducers, we focused on senescence-associated nuclear morphological changes as readout using high-throughput fluorescent microscopy (Figure 1A). We chose IMR90 human diploid fibroblasts (HDFs), which are generally more sensitive to senescence than apoptosis in response to cellular stress, and have thus been well-characterized in terms of senescence (Serrano *et al.*, 1997; Narita *et al.*, 2003). To optimize the protocol for image acquisition and the analyses of nuclear size and nuclear foci (spots), we used normal and $HRAS^{G12V}$-induced senescent (RIS) cells, which exhibit prominent senescence-associated heterochromatic foci (SAHFs) (Figure 1B) (Narita *et al.*, 2003). Cells were plated on 96-well plates, fixed, and stained with DAPI for the automated imaging of nuclei (Supplemental Figure S1, Supplemental Table S1).

Using this system we treated normal proliferating IMR90 cells with 160 kinase inhibitors (InhibitorSelect, Calbiochem/Merck) and both the nuclear size and the area of any subnuclear foci per nucleus were quantified (Figure 1C). The scores from each well were normalized to those from the DMSO controls, and the hits were determined by setting a threshold of either 1.2-fold ('relative nuclear average area') or 3-fold ('relative spot total area per nucleus') above the control. 11 and 17, out of 160 compounds (tested at a standardized 5 μM), scored positive for nuclear size (large) and spottiness (spotty), respectively, with a substantial overlap (Figure 1D, Supplemental Table S2). Cells with an enlarged or spotty nucleus tended to show a low 'relative object count per field', which reflected the averaged cell density in the area scanned (Supplemental Figure

S1C), suggesting that those hit compounds have an anti-proliferative and/or pro-cell death activity. Similar results were obtained when we treated cells with the compounds at 3 μM (Supplemental Figure S1D).

We also manually scored all the compounds by visually inspecting the scanned images. The nuclei from the cells treated with the 11 'size hits' were all recognized as substantially enlarged, and the spotty nuclei in at least 8 of 17 hits-treated cells were confirmed by eye. Interestingly, in most of the size hits, the nuclei exhibited a severe malformation with a fragmented, cashew nut-like, or doughnut-like morphology, often accompanied by multiple micronuclei ('Type I'), or a milder phenotype ('Type II') (Figure 1E, Supplemental Figure S1E). The size hits also included nuclei without any apparent irregularity ('Large'). We termed the hit compounds that induced an irregular nuclear shape and spotty morphologies IRG and SPT, respectively, and examined whether these phenotypes are associated with cellular senescence.

Hit compounds identified by the screen are capable of inducing cellular senescence

To determine whether the hit compounds induce senescence in IMR90 cells, secondary assays were performed for a subset of compounds: those that scored positive as well as those that showed a stronger irregular phenotype (Type I) in the screen (Figure 2). To optimize the doses of compounds for senescence induction, we tested different concentrations of the compounds and chose the doses that did not induce substantial cell death (Figure 2A, Supplemental Figure S1F). Cells were exposed to these compounds for 4 days (d4), followed by a further incubation without the compounds for 5 days (d9) to examine the phenotype irreversibility, a critical feature of senescence.

We confirmed that the majority of IRG-treated cells exhibited enlarged and irregular-shaped nuclei after 4-days treatment, and these nuclear phenotypes were maintained after the compounds had been removed (Figure 2A, Supplemental Figure S2). IRGs also induced a stable cell cycle arrest, as determined by a reduction in Cyclin A2, the phosphorylation status of RB (Figure 2B), and BrdU incorporation (Figure 2C); even after compound removal. Consistently, the number of colony forming cells after two weeks' incubation with compound-free medium was strongly reduced if they were pre-treated with IRGs (Figure 2D), reinforcing the long-term nature of the observed cell cycle arrest. To further confirm that the IRGs induce senescence, we measured senescence-associated ß-galactosidase (SA-ß-gal) activity, a hallmark of senescence (Dimri *et al.*, 1995). Cells pre-treated with the IRGs typically showed an enlarged cellular morphology with increased SA-ß-gal activity (Figure 2E). Although the levels of p16, a senescence-associated CDK inhibitor, were unaltered, p53 and its target p21 (another CDK inhibitor), both of which play important roles in senescence in some contexts (Chang *et al.*, 2000; 2002), were stably upregulated in IRG-treated cells (Figure 2B). Interestingly, the levels of HMGA2, a senescence marker associated with SAHFs (Funayama *et al.*, 2006; Narita *et al.*, 2006), were increased only at the later time point. Consistently, SAHF formation was also more evident at d9 (Figure 2F), thus senescence is progressively established even during the compound-free period. These results suggest that senescence is not an immediate outcome of the treatment, but rather a delayed phenotype. These compounds also induced senescence in BJ cells (another HDF), although some compounds induced a milder phenotype than in IMR90 cells (Supplemental Figure S3).

Similarly to IRGs, we also tested selected SPT hits in the secondary senescence assays. These compounds were more toxic than the IRGs and we used a lower concentration for our validation experiments. At the concentrations used (Figure 3A), the viability of cells 24h after drug treatment was >90% (Supplemental Figure S1F). Although the nuclear phenotype was relatively modest compared to the IRG hits, the formation of DAPI foci (morphologically similar to SAHFs) were significantly increased after treatment the SPT hit compounds (Figure 3A). In addition, cells pre-treated with these compounds were stably arrested, and displayed hallmark features of senescence (Figure 3, B-E). Together, our data provide a proof of principle that the nuclear phenotypes can be utilized as readout for pro-senescence screens. For the further validation of the compounds and nuclear phenotypes in the context of senescence in this study, we decided to focus on IRGs and their associated phenotype, which were strong and highly distinctive.

IRG compounds induce premature exit from M phase and tetraploidization

To examine at which cell cycle stage the IRG-treated cells accumulate and become senescent, cell cycle profiles as well as the expression pattern of cyclins were analyzed by laser scanning cytometer and immunoblotting, respectively. Following treatment with IRGs, the number of cells with a 4n DNA content became markedly increased, compared to mock-treated cells (Figure 4A). In addition there was a slight increase in the number of cells with an 8n DNA content. Interestingly, immunoblot analysis showed that those cyclins enriched in G2 or M phase (Cyclin A2 or B1, respectively) were decreased whereas a G1 cyclin (Cyclin D1) was increased during IRG-induced senescence (Figure 4B). These data suggest that the increased 4n DNA content reflects cell cycle arrest in a pseudo-G1 phase after a failed mitosis (i.e. a tetraploid state), rather than G2 arrest. This is highly reminiscent of Aurora kinase B (AURKB) inhibitors, which have been shown to induce irregular-shaped nuclear formation with polyploidization (Ditchfield *et al.*, 2003; Hauf *et al.*, 2003). Indeed, the IRGs included some compounds (Aurora kinase inhibitor II and SU6656) that can inhibit Aurora kinases (Bain *et al.*, 2007). Therefore, we tested whether the inhibition of AURKB activity by ZM1 (ZM447439) (Girdler *et al.*, 2006), a well-established AURKB inhibitor, causes cellular senescence in HDFs. Treatment of both IMR90 and BJ cells with ZM1 phenocopied the IRGs effect. Consistent with the previous studies, ZM1 treatment induced tetraploidy with a highly irregular nuclear shape (Figure 4, A-C). Detailed senescence assays confirmed that ZM1-pretreated cells exhibited a stable exit from the cell cycle with increased senescence markers (Figure 4C). Similarly to cells exposed to IRG compounds, ZM1-treated cells ceased to proliferate by d4, at which point they had irregular nuclei and were mostly tetraploid. However, the establishment of senescence again appeared to be delayed, steadily developing beyond the 4d treatment (Figure 4C, see SAHF count and HMGA2 blotting). Together, these data suggest that IRG compounds may induce senescence at least in part through, directly or indirectly, inhibiting AURKB activity.

To directly confirm the correlation between irregular nuclei and tetraploidy, the fate of mitotic nuclei was tracked by live-cell imaging of cells expressing H2B:EYFP, which had been treated with the compounds. As shown in Figure 4D, cells treated with the compounds entered M phase and condensed their chromosomes, yet they eventually decondensed without proper segregation and formed mostly single and irregular-shaped nuclei (Figure 4D, Supplemental Movies S1-S3, and data not shown). These data suggest that the irregular-shaped nuclei arise immediately after M phase without proper chromosome segregation and that cell cycle arrest at the G1 tetraploid phase is maintained during senescence development in normal HDFs.

Premature exit from M phase without chromosome segregation takes place after prolonged mitosis (mitotic slippage) (Gascoigne and Taylor, 2009) or when the spindle checkpoint is restrained (Vitale *et al.*, 2011). Inhibition of microtubule dynamics by paclitaxel (taxol, a microtubule stabilizing agent) activates the mitotic checkpoint to keep cells arrested at the metaphase/anaphase boundary, at which the well-known mitosis markers Histone H3 phosphorylated at serine 10 (H3S10ph), a direct substrate of AURKB, and Cyclin B accumulate (Figure 4E, lane 2). It has been shown that treatment with AURKB inhibitors overrides the paclitaxel-induced SAC (Ditchfield *et al.*, 2003; Hauf *et al.*, 2003). To test whether treatment with the IRGs also cancels the paclitaxel-induced SAC, we synchronized IMR90 cells with paclitaxel treatment for 12 hours, and then cells were released into paclitaxel with or without IRGs or ZM1 (Figure 4E). Similar to ZM1 (Figure 4E, lane 9), the paclitaxel-induced checkpoint was rapidly cancelled by the addition of each of the IRGs (Figure 4E, lanes 4-8), while the accumulation of Cyclin B1 and H3S10ph was virtually unaffected by the treatment with SPTs (lanes 10-12, Supplemental Figure S4). These results further support our hypothesis that treatment with the IRGs induces the irregular nuclear phenotype with tetraploidization through AURKB inhibition.

It has been shown that AURKB inhibition does not cause a substantial effect on the viability of non-proliferating cells (Ditchfield *et al.*, 2003; Hardwicke *et al.*, 2009). To ask whether cell cycle progression is required for IRGs to induce senescence, we treated quiescent IMR90 cells, induced by serum starvation, with the compounds for 3 days

(Supplemental Figure S5A). We then released the compound-treated cells from quiescent arrest into compound-free normal medium (10% serum). The pre-treated cells (during quiescence) failed to change their nuclear morphology (Supplemental Figure S5A, B) and exhibited virtually no reduction in their proliferative capacity (Supplemental Figure S5C). Therefore, IRGs and ZM1 induce senescence in proliferating, but not in non-proliferating cells. Together, these results suggest that, while these compounds have multiple targets, the downstream effects may converge on AURKB, which appears to be the dominant pathway for their senescence inducing activity.

Specific inhibition of Aurora B kinase activity triggers formation of irregular-shaped nuclei and cellular senescence

We next tested whether the IRGs directly inhibit AURKB kinase activity using a biochemical kinase profiling assay. Consistent with the phenotypic similarity between IRGs and ZM1 treatment, all five IRGs exhibited a substantial inhibitory effect against AURKA and AURKB with stronger effects on AURKB, whereas the SPT hits showed virtually no effect on the activities of the AURKs (Figure 5A). Although ZM1-induced polyploidization has been attributed to AURKB inhibition (Ditchfield *et al.*, 2003; Hauf *et al.*, 2003; Girdler *et al.*, 2006), ZM1 also inhibits AURKA, which has both a very distinct localization pattern and functions from AURKB, and, in addition to the AURKs, IRGs have multiple targets.

To specifically suppress the AURKB activity, we next sought to apply either a stable RNAi or dominant negative approach. Using a micro-RNA (miR30) based design (Silva *et al.*, 2005), we identified at least two *sh-AURKB* constructs, which substantially down-regulated the endogenous levels of AURKB and induced comparable phenotypes in IMR90 cells when stably transduced (Supplemental Figure S6). We also generated retroviral constructs encoding either an EGFP-tagged wild-type or a kinase-dead AURKB mutant (AURKB^{D218N}), which has previously been shown to function in a dominant-negative fashion (Girdler *et al.*, 2006). Endogenous AURKB levels were also down-regulated in cells expressing AURKB^{D218N} or treated with ZM1 (Figure 5B), perhaps due to the cell cycle arrest in pseudo G1 phase caused by AURKB inhibition (Gully *et al.*, 2012). Immunoblot analysis showed that expression of AURKB^{D218N} or *sh-AURKB-1*, or ZM1 treatment resulted in a reduction in H3S10ph (a substrate of AURKB), although cells expressing *sh-AURKB-1* exhibited residual AURKB activity (Figure 5B). Cyclin A2, Cyclin B1, and phosphorylated RB were down-regulated, whereas Cyclin D1 (a G1 cyclin) was increased in AURKB^{D218N} or *sh-AURKB-1* expressing cells, as observed in IRGs/ZM1-treated cells (Figure 5B, also Figure 4B). The nuclear phenotype with irregular shape was comparable between AURKB^{D218N} expressing cells and ZM1-treated cells, whereas *sh-AURKB-1* expressing cells showed a milder phenotype (Figure 5C). In addition, the senescence phenotype was also milder in the *sh-AURKB-1* expressing cells (Figure 5, B-D), implying a negative correlation between the AURKB activity and senescence phenotype (see also Supplemental Figure S6, A and B). Together, these results indicate that AURKB inhibition-induced senescence progressively develops in tetraploid cells with a highly irregular nuclear morphology and that it is an immediate consequence of AURKB inhibition in normal HDFs.

IRG compounds block the proliferation of cancer cells

AURKB inhibition in tumour cells leads to increased polyploidy, and cell cycle arrest or cell death depending on the cell type or context (Ditchfield *et al.*, 2003; Hauf *et al.*, 2003; Gizatullin *et al.*, 2006; Wilkinson *et al.*, 2007; Yang *et al.*, 2007). For example, it has been shown that in the presence of AURKB inhibitors, HeLa cervical carcinoma cells enter and exit mitosis normally, but fail to divide (Ditchfield *et al.*, 2003; Hauf *et al.*, 2003). However, long-term senescence development in tumour cells pre-treated with AURK inhibitors remains to be determined. To test whether these compounds cause therapy-induced senescence (TIS) in tumour cells, we treated HeLa cells with selective IRGs as well as ZM1. We first confirmed that cells were mostly viable (~80% at day 9, Supplemental Figure S7A) after treatment with the compounds at the concentrations used. Consistent with the phenotype of AURKB inhibition, after a 4-day treatment with these compounds the cells contained remarkably enlarged and highly irregular/multi-lobulated nuclei, or often they had numerous nuclei per cell (Figure 6A). At this stage, the cells showed only a modest retardation of cell cycle progression with little sign of senescence (probed through phosphorylation status of RB and BrdU incorporation) (Figure 6, B and C). This is perhaps consistent with the previous studies suggesting that deficiencies in the p53-p21 pathway enhance the endoreduplication caused by aurora kinase inhibitors (Ditchfield *et al.*, 2003; Gizatullin *et al.*, 2006; Kaestner *et al.*, 2009). Although HeLa cells express a, functional, wild-type p53, its level is down-regulated by human papillomavirus (HPV) E6. After an additional 5-day incubation in compound-free medium, however, cells exhibited an accumulation of the G1-cyclin (Cyclin D1) and reduced markers of cell cycle progression, such as the S/G2-cyclin (Cyclin A2), phosphorylated forms of RB, and BrdU incorporation (Figure 6, B and C), suggesting that the compound pre-treated cells eventually arrest at a pseudo-G1 phase. These cells also showed a robust accumulation of SA-ß-Gal activity (Figure 6, D and E). Thus the IRG compounds can induce senescence in HeLa cells. Their long-term arrest was confirmed by a colony formation assay in compound-free medium (Figure 6F). Interestingly, we found up-regulation of the p53-p21 pathway and HMGA2 to be delayed (Figure 6B), reinforcing the progressive nature of senescence establishment after removal of the compounds.

Since, in HeLa cells, p53 can escape from its E6-mediated down-regulation upon stress in some contexts (Wesierska-Gadek *et al.*, 2002), we next asked whether these compounds induce senescence in tumour cells that completely lack p53; using H1299, the p53-null human lung cancer cell line. While some rounded-up or floating cells were observed at both d4 and d9, IRG-treated H1299 cells were largely viable (Supplemental Figure S7B). Similarly to HeLa cells, the cells which were attached exhibited highly enlarged irregular/lobulated nuclei and/or a multinuclear phenotype (Figure 7A), the progressive accumulation of G1-cyclin (Cyclin D1) (Figure 7B), and a significant reduction in BrdU incorporation (Figure 7C), suggesting that the IRGs/ZM1 pre-treated cells also develop the pseudo-G1 phenotype. Although the reduction in DNA synthesis and Cyclin A2 levels was less pronounced than in HeLa cells at d9, the pre-treated H1299 cells showed a strong senescence-like phenotype (Figure 7D) with a marked reduction in their colony forming capacity, likely due to a combination of senescence and cell death (Figure 7E). Altogether our data suggest that AURKB inhibition triggers senescence and that this senescence develops whilst the cells are in a tetraploid state or in the case of the tumour cells, with reduced or defective p53, a polyploid state.

DISCUSSION

While the primary endpoint of conventional chemotherapy is generally cell death, senescence is gaining increasing attention as an alternative goal in cancer therapy (Acosta and Gil, 2012; Cairney *et al.*, 2012). Senescence is a heterogeneous and collective phenotype mediated by multiple effector programs, which are often associated with distinct senescence markers (Salama *et al.*, 2014). Thus this predicts the benefit of using diverse markers as a readout in screens for senescence inducers and/or senescence bypass. For example, in our screens for nuclear/chromatin morphological alterations, we identified multiple compounds that induce 'tetraploid senescence', likely through a direct inhibition of AURKB in a progressive manner. Indeed, we observed a small increase in the 8n cell population in conventional RAS-induced senescent cells (Supplemental Figure S1), suggesting that our screen also allowed the enrichment, or 'purification', of certain sub-types of the senescence phenotype. Although, as a proof of principle, we used normal HDFs, which are highly prone to senescence, and a kinase inhibitor library with a modest specificity and diversity (160 inhibitors), some of the hits were capable of inducing senescence in tumour cell lines. Thus the system is potentially applicable to TIS-screening, with a higher throughput and/or different types of libraries.

The Aurora kinases are overexpressed in a wide range of human cancers, and they are considered as promising therapeutic targets and a number of clinical trials are currently at various stages (Keen and Taylor, 2004; Green *et al.*, 2011; Goldenson and Crispino, 2014). These studies are aimed at inducing cell death and the induction of a senescence-like response has not been considered in these trials.

Inhibition of AURKB, the catalytic component of the chromosome passenger complex, overrides the SAC, which thus induces a premature exit from mitosis and interferes with cytokinesis, leading to tetraploid/binuclear cells (Keen and Taylor, 2009). However, how AURKB inhibition develops into a senescence phenotype in a tetraploid condition remains to be elucidated. In addition to an altered SAC, tetraploidization can also be induced by mitotic slippage after: a prolonged mitosis, cytokinesis failure, endoreduplication, telomere dysfunction, DNA damaging agents, or cell fusion (Storchova and Kuffer, 2008; Davoli *et al.*, 2010; Davoli and de Lange, 2011; Panopoulos *et al.*, 2014). In addition, it was recently shown that 'mitotic skip' is involved in tetraploid senescence, particularly induced by DNA damage, where p53 activation during G2 plays a key role, although any functional relation between tetraploidization and senescence was not examined (Johmura *et al.*, 2014; Krenning *et al.*, 2014). Tetraploid cells, which possess two sets of homologous chromosomes, are suggested to be genetically unstable and have a risk of producing aneuploidy, a hallmark of cancer cells (Fujiwara *et al.*, 2005; Ganem *et al.*, 2007; Storchova and Kuffer, 2008; Davoli *et al.*, 2010). It is therefore possible that normal diploid cells have mechanisms to block the further expansion of tetraploid cells. It was previously proposed that there is a p53-dependent G1 'tetraploidy checkpoint', which senses an excessive number of chromosomes or centrosomes (Andreassen *et al.*, 2001; Margolis *et al.*, 2003), although several subsequent reports have shown that a significant population of tetraploid cells can re-enter the cell cycle under optimal culture conditions (Uetake and Sluder, 2004; Wong and Stearns, 2005; Hayashi and Karlseder, 2013). Thus the existence of the tetraploidy checkpoint has been controversial. Interestingly, however, Ganem *et al.* recently showed that tetraploidization can trigger a 'G1 arrest' without an apparent DNA damage response, through the activation of the Hippo and p53 pathways (Ganem *et al.*, 2014). It would be very interesting to test whether AURKB inhibition-induced senescence is, at least in part, dependent on these pathways.

Our data suggest that senescence is a delayed process rather than an immediate consequence of tetraploidization. We also found that the senescence phenotype can still progress after AURKB inhibition in p53-defective cells, where cells can undergo endoreduplication, leading a highly polyploid senescence (Figures 6 and 7). Thus, although extra numbers of chromosomes might contribute to inducing senescence, particularly in normal cells, it is also possible that the pathophysiology behind polyploidization can provoke senescence effector mechanisms. Indeed, both senescence and tetraploidy are associated with some common pathophysiological contexts, including wound healing, ageing, and pre-neoplasia (Ermis *et al.*, 1998; Ganem *et al.*, 2007; Davoli and de Lange, 2011; Gentric *et al.*, 2012). In addition, it was recently shown that cell fusion can also induce senescence (Chuprin *et al.*, 2013). In all conditions, genotoxic stress or DNA damage response (DDR) is involved in senescence (Bartkova *et al.*, 2006; Di Micco *et al.*, 2006; Davoli *et al.*, 2010; Jun and Lau, 2010; Chuprin *et al.*, 2013; López-Otín *et al.*, 2013).

While senescence involves diverse effector mechanisms, a persistent DDR is proposed to be a widespread mechanism behind senescence induction in diverse types of stress (Bartkova *et al.*, 2006; Di Micco *et al.*, 2006; Mallette *et al.*, 2007; d'Adda di Fagagna, 2008; Rodier *et al.*, 2009). Interestingly, mitotic errors can cause lagging chromosomes, leading to formation of micronuclei, which are associated with DNA damage (Guerrero *et al.*, 2010; Thompson and Compton, 2011; Crasta *et al.*, 2012). For example, it was shown that cells bearing a mutated *death inducer obliterator* (*Dido*) gene, which causes

SAC dysregulation, show DNA damage localized at their centromeric regions, particularly in micronuclei, which are derived via a mitotic defect (Guerrero *et al.*, 2010). Unlike DNA damage in telomeric regions, which is not readily reparable (Fumagalli *et al.*, 2012; Hewitt *et al.*, 2012; Suram *et al.*, 2012) and avoids end detection (Carneiro *et al.*, 2010), centromeric DNA damage appears to be reparable (Guerrero *et al.*, 2010). However, in addition to telomeric regions, senescence associated-persistent DNA damage (collectively called 'DNA-SCARS') can also be observed within the bodies of chromosomes, although the mechanism for the failed DNA repair in these regions remains to be determined (Rodier *et al.*, 2011). It was also shown that micronuclei contain aberrant DNA replication-associated DNA damage, which can persist during G2, particularly in p53-deficient conditions (Crasta *et al.*, 2012). We confirmed that the micronuclei caused by IRGs/ZM1 treatment at d4 were often positive for both γH2AX (a DNA damage marker) and centromere protein A (CENPA) in HDFs (Supplemental Figure S8). Such DNA damage may provoke other senescence effectors, contributing to the progressive development of senescence.

It has been proposed that mitotic failure can lead shortly afterwards to a distinct form of cell death. This process is called 'mitotic catastrophe', but it involves as yet poorly understood mechanisms (Vitale *et al.*, 2011; Hayashi and Karlseder, 2013). In addition to cell death, senescence has also been implicated in this process (Shay and Roninson, 2004; Vitale *et al.*, 2011; Hayashi and Karlseder, 2013). For example, factors that dysregulate the SAC can also induce senescence, followed by eventual cell death due to mitotic catastrophe (Chang *et al.*, 2000; Eom *et al.*, 2005; Yun *et al.*, 2009). In addition, HDFs extend their replicative life span when tumour suppressors, including p53, are lost and cells escape replicative senescence, eventually undergoing a net growth arrest with a high rate of cell death (called M2 or 'crisis') likely due to mitotic catastrophe (Shay and Wright, 2005).

The relationship between senescence 'escapers' and mitotic catastrophe raises an interesting possibility, a potential mode of selective killing for 'unstable' senescent cells. Particularly in the TIS context, the incomplete establishment of senescence in tumour cells may even promote tumour development and recurrence, in part through the longer-term aspects of the non-cell-autonomous activities of senescence. Indeed, it has been shown that senescence-induction needs to be coupled with the subsequent elimination of senescent cells in order to achieve an efficient tumour suppression or pro-senescence therapeutic outcome (Xue *et al.*, 2007; Rakhra *et al.*, 2010; Kang *et al.*, 2011). Currently, the proposed mechanisms for the 'selective elimination of senescent cells' are mainly mediated through the immune response (Xue *et al.*, 2007; Krizhanovsky *et al.*, 2008; Kang *et al.*, 2011; Pérez-Mancera *et al.*, 2014), while a recent study provided evidence that senescent cells can also be eliminated through metabolic perturbation in a TIS context (Dörr *et al.*, 2013). Notably the mitotic catastrophe and cell death following senescence escape are often associated with deficiencies in the p53-p21 pathway (Chang *et al.*, 2000; Shay and Roninson, 2004; Yun *et al.*, 2009), which is often abrogated in cancer, thus reinforcing the therapeutic relevance of the pro-senescence cancer therapy of using SAC modulators. Consistently, it was recently shown that p53 deficiency sensitizes cells to the premature mitotic exit caused by AURKB inhibition (Marxer *et al.*, 2014). Also, the inhibitor of aurora kinases, VX-680, was previously shown to induce cell death preferentially in tumour cells with a compromised p53-dependent post-mitotic checkpoint, although this effect appears to be highly cell type dependent (Gizatullin *et al.*, 2006). The above is also perhaps consistent with our data that p53-null H1299 cells treated with IRGs/ZM1 showed a defective colony forming ability with a relatively mild senescence phenotype (Figure 7). While senescence has often been suggested to be a ‘back-up’ of apoptotic failure (Schmitt *et al*, 2002), such potential reciprocal back-up interactions between senescence and cell death through mitotic catastrophe might provide additional justification for AURKB inhibitors, or other SAC modulators, as a therapeutic module in cancer.

MATERIALS AND METHODS

Cell culture and gene transfer

IMR90 and BJ human fibroblasts (ATCC) were cultured in phenol-red free DMEM with 10% FBS under 5% oxygen as described previously (Young *et al.*, 2009). HeLa and H1299 cells (ATCC) were cultured in phenol-red free DMEM with 10% FBS. Retroviral gene transfer was carried out as described(Narita *et al.*, 2006). RAS-induced senescence (RIS) was triggered by the addition of 4OHT to cells expressing H-RAS^{G12V} fused to the estrogen receptor (ER) ligand-binding domain (ER:RAS)(Young *et al.*, 2009). Quiescence was induced by incubating cells in DMEM with 0.1% serum for 3 days.

Plasmids

The following retroviral plasmids were used: pLNCX2 (*ER:H-RAS*^{G12V} (*ER:RAS*)) (Young *et al.*, 2009), pWZL-hygro (*EGFP*, *EGFP:AURKB*, *EDFP:AURKB*^{D218N}). miR30-based shRNA; pMSCV-puro (*sh-AURKB*) (Silva *et al.*, 2005). The following target sequences were used for pMSCV-miR30-*AURKB*: gaagggatccctaactgtt (#1), tttgtttaataaaggctga (#2), ggtccctgtcattcactcg (#3), and actgttcccttatctgtt (#4)

Antibodies

Antibodies used for Western blotting were as follows: Cyclin A2 (C4710, Sigma), Cyclin B1 (4135, Cell Signaling), Cyclin D1 (2926, Cell Signaling), p16 (sc-759, Santa cruz), p21 (sc-397, Santa Cruz), p53 (sc-126, Santa Cruz), HMGA2 (sc-30223, Santa Cruz), H3S10phos (ab14955, Abcam), Histone H3 (ab1791, Abcam), AURKB (ab2254, Abcam), ß-actin (A5441, Sigma), Rb (9309, Cell Signaling).

Compound screening

IMR90 cells were plated in a 96-well plate (353948, BD Falcon) at 10,000 cells per well. After 24 hours, the medium was replaced by those containing 3 μM or 5 μM kinase inhibitors (InhibitorSelect kinase inhibitor library including 160 compounds, Calbiochem/Merck). 4 days after compound addition, cells were washed with PBS, fixed in PBS with 4% paraformaldehyde for 15 min, and washed with PBS three times. Fixed cells were stained with 1 μg/ml DAPI in PBS (+0.2% Triton X-100) for 5 min. Images of the nuclei were captured and analyzed by ArrayScan (Thermo Scientific) with the settings shown in Table S1. Briefly, nuclear contour was first determined (channel 1) and then spotty structures overlapping with the nuclei were identified (channel 2). To rank the compounds by nuclear size and spottiness, the parameters 'Relative nuclear average area' and 'Relative spot total area per nucleus' over DMSO control were used for the analyses, respectively. The compounds that gave less than a count of 100 nuclei per well were categorized as 'Toxic' and excluded from analyses. Hit compounds from each category were further narrowed down and re-categorized by visual inspection.

Compounds

The final concentrations used for each individual compound was as follows. For HDFs and H1299 cells, Aurora kinase inhibitor II: 8 μM (CAS# 331770-21-9; 189404, Merck); Cdk2 inhibitor IV, NU6140: 4 μM (CAS# 444723-13-1; 238804, Merck); PDGFR tyrosine kinase inhibitor V: 8 μM (CAS# 347155-76-4; 521234, Merck); Rho kinase inhibitor IV: 10 μM (555554, Merck or CAS# 913844-45-8; 2485, Tocris); SU6656: 10 μM (CAS# 330161-87-0; 572635, Merck); ZM1 (ZM-447439): 2 μM (CAS# 331771-20-1; sc-200696, Santa Cruz); EGFR inhibitor: 0.5 μM (CAS# 879127-

07-8; 324674, Merck); JNK inhibitor IX: 0.5 μM (CAS# 312917-14-9; 420136, Merck); MK2a inhibitor: 0.7 μM (CAS# 41179-33-3; 475863, Merck). For HeLa cells, Rho kinase inhibitor IV, Cdk2 inhibitor IV and ZM1 were used at the concentration of 1.5, 4 and 1.5 μM, respectively. Nocodazole: 200 ng/ml (CAS# 31430-18-9; 487928, Merck); Paclitaxel: 10 μM (CAS# 33069-62-4; T7402, Sigma).

Senescence and viability assays

Cells were treated with the hit compounds for 4 days (d4), followed by 5 days incubation in compound-free media (d9) unless stated. BrdU incorporation, SA-ß-gal and colony formation assays were conducted as described(Narita *et al.*, 2003). Primary antibody for BrdU incorporation: 555627, Becton Dickinson. Cell viability was determined by trypan blue exclusion.

Immunofluorescence and laser scanning cytometer (LSC)

Immunofluorescence was performed as described (Narita *et al.*, 2003). Primary antibodies: H3K9me3 (07-523, Millipore), H3K36me3 (13C9) (Chandra *et al.*, 2012), LMNA (sc-20680, Santa Cruz), α-Tubulin (T5168, Sigma). Images were acquired with confocal (when stated) or wide-field fluorescence microscopy. LSC (Compucyte iCys) was used to determine cell cycle profile and nuclear size distribution.

Live cell imaging

IMR90 cells stably expressing Histone H2B:EYFP were synchronized at the G1/S border using a double thymidine treatment. Briefly, cells were plated at a density of 1.76×10^4 cells (in 300 μl medium) per well on to an 8 well μ-slide (80826, ibidi). One day after plating, the medium was replaced with that containing 2 mM thymidine and incubated for 14 hours. Cells were washed three times with pre-warmed 200 µl PBS and released into thymidine-free medium for 12 hours. Then cells were again incubated 13 hours in the medium containing thymidine. These synchronized cells were washed three times with pre-warmed 200 µl PBS and released into medium containing the compounds. 10 hours later, imaging was started and continued for ~5 hours (5 min interval) with Eclipse TE2000 PFS Color microscope (Nikon). Conditions for the imaging were as follows: x10 objective; three focal planes, 3 µm apart; three fields per well; exposure time (bright field: 20 ms; YFP: 400 ms); gain: 13.6x; ND filter: 1. Movie and individual files were processed by NIS-Elements software and ImageJ 1.48s.

In vitro kinase assay

The IC_{50} of the compounds was identified using a Z'-LYTE *in vitro* kinase assay and was carried out by the SelectScreen biochemical kinase profiling service (Invitrogen). The assay was conducted at ten points from 1 nM up to 2 mM with the ATP concentration shown: 10 µM for AURKA; 81µM for AURKB.

ACKNOWLEDGMENTS

The authors thank F. Gergely, VM Draviam, T. Toda, and P. Parker for their thoughtful discussions, SH Lee for critical reading and discussions; CI core Microscopy facility (A. Schreiner, H. Zecchini, and L. Berry) and CRT discovery laboratory for technical support. This work was supported by the University of Cambridge, Cancer Research UK, Hutchison Whampoa; Cancer Research UK grants A6691 and A9892 (M.N., N.K., C.J.T., D.C.B., C.J.C., L.S.G, and M.S.); a fellowship from the Uehara Memorial Foundation (M.S.).

REFERENCES

Acosta, J. C. *et al.* (2008). Chemokine signaling via the CXCR2 receptor reinforces senescence. Cell *133*, 1006–1018.

Acosta, J. C., and Gil, J. (2012). Senescence: a new weapon for cancer therapy. Trends Cell Biol. *22*, 211–219.

Andreassen, P. R., Lohez, O. D., and Lacroix, F. B. (2001). Tetraploid state induces p53-dependent arrest of nontransformed mammalian cells in G1. Mol. Biol. Cell *12*, 1315–1328.

Bain, J., Plater, L., Elliott, M., Shpiro, N., Hastie, C. J., McLauchlan, H., Klevernic, I., Arthur, J. S. C., Alessi, D. R., and Cohen, P. (2007). The selectivity of protein kinase inhibitors: a further update. Biochem. J. *408*, 297–315.

Barascu, A., Le Chalony, C., Pennarun, G., Genet, D., Imam, N., Lopez, B., and Bertrand, P. (2012). Oxidative stress induces an ATM-independent senescence pathway through p38 MAPK-mediated lamin B1 accumulation. EMBO J. *31*, 1080–1094.

Bartkova, J., Rezaei, N., Liontos, M., and Karakaidos, P. (2006). Oncogene-induced senescence is part of the tumorigenesis barrier imposed by DNA damage checkpoints. Nature *444*, 633–637.

Bemiller, P. M., and Lee, L. H. (1978). Nucleolar changes in senescing WI-38 cells. Mech. Ageing Dev. *8*, 417–427.

Bischof, O., Kirsh, O., Pearson, M., Itahana, K., Pelicci, P. G., and Dejean, A. (2002). Deconstructing PML-induced premature senescence. EMBO J. *21*, 3358–3369.

Bischof, O., Nacerddine, K., and Dejean, A. (2005). Human papillomavirus oncoprotein E7 targets the promyelocytic leukemia protein and circumvents cellular senescence via the Rb and p53 tumor suppressor pathways. Mol. Cell. Biol. *25*, 1013–1024.

Cairney, C. J., Bilsland, A. E., Evans, T. R. J., Roffey, J., Bennett, D. C., Narita, M., Torrance, C. J., and Keith, W. N. (2012). Cancer cell senescence: a new frontier in drug development. Drug Discov. Today *17*, 269–276.

Campisi, J. (2013). Aging, cellular senescence, and cancer. Annu. Rev. Physiol. *75*, 685–705.

Carmena, M., Wheelock, M., Funabiki, H., and Earnshaw, W. C. (2012). The chromosomal passenger complex (CPC): from easy rider to the godfather of mitosis. Nat. Rev. Mol. Cell Biol. *13*, 789–803.

Carneiro, T., Khair, L., Reis, C. C., Borges, V., Moser, B. A., Nakamura, T. M., and Ferreira, M. G. (2010). Telomeres avoid end detection by severing the checkpoint signal transduction pathway. Nature *467*, 228–232.

Chandra, T. *et al.* (2012). Independence of Repressive Histone Marks and Chromatin Compaction during Senescent Heterochromatic Layer Formation. Mol. Cell *47*, 203–214.

Chang, B. D., Broude, E. V., Fang, J., Kalinichenko, T. V., Abdryashitov, R., Poole, J. C., and Roninson, I. B. (2000). p21Waf1/Cip1/Sdi1-induced growth arrest is associated with depletion of mitosis-control proteins and leads to abnormal mitosis and endoreduplication in recovering cells. Oncogene *19*, 2165–2170.

Chang, B.-D., Swift, M. E., Shen, M., Fang, J., Broude, E. V., and Roninson, I. B. (2002). Molecular determinants of terminal growth arrest induced in tumor cells by a chemotherapeutic agent. Proc. Natl. Acad. Sci. U.S.A. *99*, 389–394.

Chuprin, A., Gal, H., Biron-Shental, T., Biran, A., Amiel, A., Rozenblatt, S., and Krizhanovsky, V. (2013). Cell fusion induced by ERVWE1 or measles virus causes cellular senescence. Genes Dev. *27*, 2356–2366.

Coppé, J.-P., Desprez, P.-Y., Krtolica, A., and Campisi, J. (2010). The senescence-associated secretory phenotype: the dark side of tumor suppression. Annu. Rev. Pathol. *5*, 99–118.

Correia-Melo, C., Hewitt, G., and Passos, J. F. (2014). Telomeres, oxidative stress and inflammatory factors: partners in cellular senescence? Longev. Healthspan *3*, 1.

Crasta, K., Ganem, N. J., Dagher, R., Lantermann, A. B., Ivanova, E. V., Pan, Y., Nezi, L., Protopopov, A., Chowdhury, D., and Pellman, D. (2012). DNA breaks and chromosome pulverization from errors in mitosis. Nature.

Cristofalo, V. J., and Pignolo, R. J. (1993). Replicative senescence of human fibroblast-like cells in culture. Physiol. Rev. *73*, 617–638.

d'Adda di Fagagna, F. (2008). Living on a break: cellular senescence as a DNA-damage response. Nat. Rev. Cancer *8*, 512–522.

Davoli, T., and de Lange, T. (2011). The causes and consequences of polyploidy in normal development and cancer. Annu. Rev. Cell Dev. Biol. *27*, 585–610.

Davoli, T., Denchi, E. L., and de Lange, T. (2010). Persistent telomere damage induces bypass of mitosis and tetraploidy. Cell *141*, 81–93.

Di Micco, R. *et al.* (2006). Oncogene-induced senescence is a DNA damage response triggered by DNA hyper-replication. Nature *444*, 638–642.

Dimri, G. P., Lee, X., Basile, G., Acosta, M., Scott, G., Roskelley, C., Medrano, E. E., Linskens, M., Rubelj, I., and Pereira-Smith, O. (1995). A biomarker that identifies senescent human cells in culture and in aging skin in vivo. Proc. Natl. Acad. Sci. U.S.A. *92*, 9363–9367.

Ditchfield, C., Johnson, V. L., Tighe, A., Ellston, R., Haworth, C., Johnson, T., Mortlock, A., Keen, N., and Taylor, S. S. (2003). Aurora B couples chromosome alignment with anaphase by targeting BubR1, Mad2, and Cenp-E to kinetochores. J. Cell Biol. *161*, 267–280.

Dörr, J. R. *et al.* (2013). Synthetic lethal metabolic targeting of cellular senescence in cancer therapy. Nature *501*, 421–425.

Dreesen, O. *et al.* (2013). Lamin B1 fluctuations have differential effects on cellular proliferation and senescence. J. Cell Biol. *200*, 605–617.

Eom, Y.-W., Kim, M. A., Park, S. S., Goo, M. J., Kwon, H. J., Sohn, S., Kim, W.-H., Yoon, G., and Choi, K. S. (2005). Two distinct modes of cell death induced by doxorubicin: apoptosis and cell death through mitotic catastrophe accompanied by senescence-like phenotype. Oncogene *24*, 4765–4777.

Ermis, A., Oberringer, M., Wirbel, R., Koschnick, M., Mutschler, W., and Hanselmann, R. G. (1998). Tetraploidization is a physiological enhancer of wound healing. Eur. Surg. Res. *30*, 385–392.

Ewald, J. A., Desotelle, J. A., Wilding, G., and Jarrard, D. F. (2010). Therapy-induced senescence in cancer. JNCI J. Natl. Cancer Inst. *102*, 1536–1546.

Ewald, J. A., Peters, N., Desotelle, J. A., Hoffmann, F. M., and Jarrard, D. F. (2009). A high-throughput method to identify novel senescence-inducing compounds. J. Biomol. Screen *14*, 853–858.

Ferbeyre, G., de Stanchina, E., Querido, E., Baptiste, N., Prives, C., and Lowe, S. W. (2000). PML is induced by oncogenic ras and promotes premature senescence. Genes Dev. *14*, 2015–2027.

Freund, A., Laberge, R.-M., Demaria, M., and Campisi, J. (2012). Lamin B1 loss is a senescence-associated biomarker. Mol. Biol. Cell *23*, 2066–2075.

Fujiwara, T., Bandi, M., Nitta, M., Ivanova, E. V., Bronson, R. T., and Pellman, D. (2005). Cytokinesis failure generating tetraploids promotes tumorigenesis in p53-null cells. Nature *437*, 1043–1047.

Fumagalli, M. *et al.* (2012). Telomeric DNA damage is irreparable and causes persistent DNA-damage-response activation. Nat. Cell Biol. *14*, 355–365.

Funayama, R., Saito, M., Tanobe, H., and Ishikawa, F. (2006). Loss of linker histone H1 in cellular senescence. J. Cell Biol. *175*, 869–880.

Ganem, N. J., Cornils, H., Chiu, S.-Y., O'Rourke, K. P., Arnaud, J., Yimlamai, D., Théry, M., Camargo, F. D., and Pellman, D. (2014). Cytokinesis failure triggers hippo tumor suppressor pathway activation. Cell *158*, 833–848.

Ganem, N. J., Storchova, Z., and Pellman, D. (2007). Tetraploidy, aneuploidy and cancer. Curr. Opin. Genet. Dev. *17*, 157–162.

Gascoigne, K. E., and Taylor, S. S. (2009). How do anti-mitotic drugs kill cancer cells? J. Cell. Sci. *122*, 2579–2585.

Gautschi, O., Heighway, J., Mack, P. C., Purnell, P. R., Lara, P. N., and Gandara, D. R. (2008). Aurora kinases as anticancer drug targets. Clin. Cancer Res. *14*, 1639–1648.

Gentric, G., Desdouets, C., and Celton-Morizur, S. (2012). Hepatocytes polyploidization and cell cycle control in liver physiopathology. Int. J. Hepatol. *2012*, 282430–282438.

Gewirtz, D. A., Holt, S. E., and Elmore, L. W. (2008). Accelerated senescence: An emerging role in tumor cell response to chemotherapy and radiation. Biochem. Pharmacol. *76*, 947–957.

Gil, J., Bernard, D., Martínez, D., and Beach, D. (2004). Polycomb CBX7 has a unifying role in cellular lifespan. Nat. Cell Biol. *6*, 67–72.

Girdler, F., Gascoigne, K. E., Eyers, P. A., Hartmuth, S., and Taylor, S. S. (2006). Validating Aurora B as an anti-cancer drug target. J. Cell. Sci. *119*, 3664–3675.

Gizatullin, F., Yao, Y., Kung, V., Harding, M. W., Loda, M., and Shapiro, G. I. (2006). The Aurora kinase inhibitor VX-680 induces endoreduplication and apoptosis preferentially in cells with compromised p53-dependent postmitotic checkpoint function. Cancer Res. *66*, 7668–7677.

Goldenson, B., and Crispino, J. D. (2014). The aurora kinases in cell cycle and leukemia. Oncogene.

Goldstein, S. (1990). Replicative senescence: the human fibroblast comes of age. Science *249*, 1129–1133.

Green, M. R., Woolery, J. E., and Mahadevan, D. (2011). Update on Aurora Kinase Targeted Therapeutics in Oncology. Expert Opin. Drug Discov. *6*, 291–307.

Guerrero, A. A., Gamero, M. C., Trachana, V., Fütterer, A., Pacios-Bras, C., Díaz-Concha, N. P., Cigudosa, J. C., Martínez-A, C., and van Wely, K. H. M. (2010). Centromere-localized breaks indicate the generation of DNA damage by the mitotic spindle. Proc. Natl. Acad. Sci. U.S.A. *107*, 4159–4164.

Gully, C. P. *et al.* (2012). Aurora B kinase phosphorylates and instigates degradation of p53. Proc. Natl. Acad. Sci. U.S.A. *109*, E1513–E1522.

Hardwicke, M. A. *et al.* (2009). GSK1070916, a potent Aurora B/C kinase inhibitor with broad antitumor activity in tissue culture cells and human tumor xenograft models. Mol. Cancer Ther. *8*, 1808–1817.

Hauf, S., Cole, R. W., LaTerra, S., Zimmer, C., Schnapp, G., Walter, R., Heckel, A., van Meel, J., Rieder, C. L., and Peters, J.-M. (2003). The small molecule Hesperadin reveals a role for Aurora B in correcting kinetochore-microtubule attachment and in maintaining the spindle assembly checkpoint. J. Cell Biol. *161*, 281–294.

Hayashi, M. T., and Karlseder, J. (2013). DNA damage associated with mitosis and cytokinesis failure. Oncogene *32*, 4593–4601.

Hewitt, G., Jurk, D., Marques, F. D. M., Correia-Melo, C., Hardy, T., Gackowska, A., Anderson, R., Taschuk, M., Mann, J., and Passos, J. F. (2012). Telomeres are favoured targets of a persistent DNA damage response in ageing and stress-induced senescence. Nat. Commun. *3*, 708.

Jacobs, J. J. *et al.* (2000). Senescence bypass screen identifies TBX2, which represses Cdkn2a (p19(ARF)) and is amplified in a subset of human breast cancers. Nat. Genet. *26*, 291–299.

Johmura, Y. *et al.* (2014). Necessary and sufficient role for a mitosis skip in senescence induction. Mol. Cell *55*, 73–84.

Jun, J.-I., and Lau, L. F. (2010). The matricellular protein CCN1 induces fibroblast senescence and restricts fibrosis in cutaneous wound healing. Nat. Cell Biol. *12*, 676–685.

Jung, J.-E. *et al.* (2005). Survivin inhibits anti-growth effect of p53 activated by aurora B. Biochem. Biophys. Res. Commun. *336*, 1164–1171.

Kaestner, P., Stolz, A., and Bastians, H. (2009). Determinants for the efficiency of anticancer drugs targeting either Aurora-A or Aurora-B kinases in human colon carcinoma cells. Mol. Cancer Ther. *8*, 2046–2056.

Kang, T.-W. *et al.* (2011). Senescence surveillance of pre-malignant hepatocytes limits liver cancer development. Nature *479*, 547–551.

Keen, N., and Taylor, S. (2004). Aurora-kinase inhibitors as anticancer agents. Nat. Rev. Cancer *4*, 927–936.

Keen, N., and Taylor, S. (2009). Mitotic drivers—inhibitors of the Aurora B Kinase. Cancer Metastasis Rev. *28*, 185–195.

Kelly, A. E., and Funabiki, H. (2009). Correcting aberrant kinetochore microtubule attachments: an Aurora B-centric view. Curr. Opin. Cell Biol. *21*, 51–58.

Kim, H.-J., Cho, J. H., Quan, H., and Kim, J.-R. (2011). Down-regulation of Aurora B kinase induces cellular senescence in human fibroblasts and endothelial cells through a p53-dependent pathway. FEBS Lett. *585*, 3569–3576.

Kortlever, R. M., Brummelkamp, T. R., van Meeteren, L. A., Moolenaar, W. H., and Bernards, R. (2008). Suppression of the p53-dependent replicative senescence response by lysophosphatidic acid signaling. Mol. Cancer Res. *6*, 1452–1460.

Krenning, L., Feringa, F. M., Shaltiel, I. A., van den Berg, J., and Medema, R. H. (2014). Transient activation of p53 in G2 phase is sufficient to induce senescence. Mol. Cell *55*, 59-72.

Krizhanovsky, V., Yon, M., Dickins, R. A., Hearn, S., Simon, J., Miething, C., Yee, H., Zender, L., and Lowe, S. W. (2008). Senescence of activated stellate cells limits liver fibrosis. Cell *134*, 657–667.

Kuilman, T., and Peeper, D. S. (2009). Senescence-messaging secretome: SMS-ing cellular stress. Nat. Rev. Cancer *9*, 81–94.

Lahtela, J., Corson, L. B., Hemmes, A., Brauer, M. J., Koopal, S., Lee, J., Hunsaker, T. L., Jackson, P. K., and Verschuren, E. W. (2013). A high-content cellular senescence screen identifies candidate tumor suppressors, including EPHA3. Cell Cycle *12*, 625–634.

Leal, J. F. M. *et al.* (2008). Cellular senescence bypass screen identifies new putative tumor suppressor genes. Oncogene *27*, 1961–1970.

Lens, S. M. A., Voest, E. E., and Medema, R. H. (2010). Shared and separate functions of polo-like kinases and aurora kinases in cancer. Nat. Rev. Cancer *10*, 825–841.

Liu, Y. *et al.* (2013). Targeting aurora kinases limits tumour growth through DNA damage-mediated senescence and blockade of NF-κB impairs this drug-induced senescence. EMBO Mol. Med. *5*, 149–166.

López-Otín, C., Blasco, M. A., Partridge, L., Serrano, M., and Kroemer, G. (2013). The Hallmarks of Aging. Cell *153*, 1194–1217.

Maeshima, K., Yahata, K., Sasaki, Y., Nakatomi, R., Tachibana, T., Hashikawa, T., Imamoto, F., and Imamoto, N. (2006). Cell-cycle-dependent dynamics of nuclear pores: pore-free islands and lamins. J. Cell. Sci. *119*, 4442–4451.

Mallette, F. A., Gaumont-Leclerc, M.-F., and Ferbeyre, G. (2007). The DNA damage signaling pathway is a critical mediator of oncogene-induced senescence. Genes Dev. *21*, 43–48.

Margolis, R. L., Lohez, O. D., and Andreassen, P. R. (2003). G1 tetraploidy checkpoint and the suppression of tumorigenesis. J. Cell. Biochem. *88*, 673–683.

Marxer, M., Ma, H. T., Man, W. Y., and Poon, R. Y. C. (2014). p53 deficiency enhances mitotic arrest and slippage induced by pharmacological inhibition of Aurora kinases. Oncogene *33*, 3550–3560.

Matsumura, T., Zerrudo, Z., and HAYFLICK, L. (1979). Senescent human diploid cells in culture: survival, DNA synthesis and morphology. J. Gerontol. *34*, 328–334.

Mitsui, Y., and Schneider, E. L. (1976). Increased nuclear sizes in senescent human diploid fibroblast cultures. Exp. Cell Res. *100*, 147–152.

Muñoz-Espín, D. *et al.* (2013). Programmed Cell Senescence during Mammalian Embryonic Development. Cell *155*, 1104–1118.

Narita, M., Narita, M., Krizhanovsky, V., Nuñez, S., Chicas, A., Hearn, S. A., Myers, M. P., and Lowe, S. W. (2006). A novel role for high-mobility group a proteins in cellular senescence and heterochromatin formation. Cell *126*, 503–514.

Narita, M., Nuñez, S., Heard, E., Narita, M., Lin, A. W., Hearn, S. A., Spector, D. L., Hannon, G. J., and Lowe, S. W. (2003). Rb-mediated heterochromatin formation and silencing of E2F target genes during cellular senescence. Cell *113*, 703–716.

Panopoulos, A., Pacios-Bras, C., Choi, J., Yenjerla, M., Sussman, M. A., Fotedar, R., and Margolis, R. L. (2014). Failure of cell cleavage induces senescence in tetraploid primary cells. Mol. Biol. Cell *25*, 3105–3118.

Pearson, M. *et al.* (2000). PML regulates p53 acetylation and premature senescence induced by oncogenic Ras. Nature *406*, 207–210.

Pérez-Mancera, P. A., Young, A. R. J., and Narita, M. (2014). Inside and out: the activities of senescence in cancer. Nat. Rev. Cancer *14*, 547–558.

Poele, te, R. H., Okorokov, A. L., Jardine, L., Cummings, J., and Joel, S. P. (2002). DNA damage is able to induce senescence in tumor cells in vitro and in vivo. Cancer Res. *62*, 1876–1883.

Rakhra, K. *et al.* (2010). CD4(+) T cells contribute to the remodeling of the microenvironment required for sustained tumor regression upon oncogene inactivation. Cancer Cell *18*, 485–498.

Rodier, F. *et al.* (2011). DNA-SCARS: distinct nuclear structures that sustain damage-induced senescence growth arrest and inflammatory cytokine secretion. J. Cell. Sci. *124*, 68–81.

Rodier, F., Coppé, J.-P., Patil, C. K., Hoeijmakers, W. A. M., Muñoz, D. P., Raza, S. R., Freund, A., Campeau, E., Davalos, A. R., and Campisi, J. (2009). Persistent DNA damage signalling triggers senescence-associated inflammatory cytokine secretion. Nat. Cell Biol. *11*, 973–979.

Rovillain, E., Mansfield, L., Lord, C. J., Ashworth, A., and Jat, P. S. (2011). An RNA interference screen for identifying downstream effectors of the p53 and pRB tumour suppressor pathways involved in senescence. BMC Genomics *12*, 355.

Sadaie, M. *et al.* (2013). Redistribution of the Lamin B1 genomic binding profile affects rearrangement of heterochromatic domains and SAHF formation during senescence. Genes Dev. *27*, 1800–1808.

Salama, R., Sadaie, M., Hoare, M., and Narita, M. (2014). Cellular senescence and its effector programs. Genes Dev. *28*, 99–114.

Schmitt, C. A., Fridman, J. S., Yang, M., Lee, S., Baranov, E., Hoffman, R. M., and Lowe, S. W. (2002). A senescence program controlled by p53 and p16INK4a contributes to the outcome of cancer therapy. Cell *109*, 335–346.

Serrano, M., Lin, A. W., McCurrach, M. E., Beach, D., and Lowe, S. W. (1997). Oncogenic ras provokes premature cell senescence associated with accumulation of p53 and p16INK4a. Cell *88*, 593–602.

Shah, P. P. *et al.* (2013). Lamin B1 depletion in senescent cells triggers large-scale changes in gene expression and the chromatin landscape. Genes Dev. *27*, 1787–1799.

Shay, J. W., and Roninson, I. B. (2004). Hallmarks of senescence in carcinogenesis and cancer therapy. Oncogene *23*, 2919–2933.

Shay, J. W., and Wright, W. E. (2005). Senescence and immortalization: role of telomeres and telomerase. Carcinogenesis *26*, 867–874.

Shvarts, A., Brummelkamp, T. R., Scheeren, F., Koh, E., Daley, G. Q., Spits, H., and Bernards, R. (2002). A senescence rescue screen identifies BCL6 as an inhibitor of anti-proliferative p19(ARF)-p53 signaling. Genes Dev. *16*, 681–686.

Silva, J. M. *et al.* (2005). Second-generation shRNA libraries covering the mouse and human genomes. Nat. Genet. *37*, 1281–1288.

Storchova, Z., and Kuffer, C. (2008). The consequences of tetraploidy and aneuploidy. J. Cell. Sci. *121*, 3859–3866.

Storer, M. *et al.* (2013). Senescence Is a Developmental Mechanism that Contributes to Embryonic Growth and Patterning. Cell *155*, 1119–1130.

Suram, A. *et al.* (2012). Oncogene-induced telomere dysfunction enforces cellular senescence in human cancer precursor lesions. EMBO J. *31*, 2839–2851.

Thompson, S. L., and Compton, D. A. (2011). Chromosome missegregation in human cells arises through specific types of kinetochore-microtubule attachment errors. Proc. Natl. Acad. Sci. U.S.A. *108*, 17974–17978.

Uetake, Y., and Sluder, G. (2004). Cell cycle progression after cleavage failure: mammalian somatic cells do not possess a "tetraploidy checkpoint". J. Cell Biol. *165*, 609–615.

Vitale, I., Galluzzi, L., Castedo, M., and Kroemer, G. (2011). Mitotic catastrophe: a mechanism for avoiding genomic instability. Nat. Rev. Mol. Cell Biol. *12*, 385–392.

Wesierska-Gadek, J., Schloffer, D., Kotala, V., and Horky, M. (2002). Escape of p53 protein from E6-mediated degradation in HeLa cells after cisplatin therapy. Int. J. Cancer *101*, 128–136.

Wilkinson, R. W. *et al.* (2007). AZD1152, a selective inhibitor of Aurora B kinase, inhibits human tumor xenograft growth by inducing apoptosis. Clin. Cancer Res. *13*, 3682–3688.

Wong, C., and Stearns, T. (2005). Mammalian cells lack checkpoints for tetraploidy, aberrant centrosome number, and cytokinesis failure. BMC Cell Biol. *6*, 6.

Xue, W., Zender, L., Miething, C., Dickins, R. A., Hernando, E., Krizhanovsky, V., Cordón-Cardo, C., and Lowe, S. W. (2007). Senescence and tumour clearance is triggered by p53 restoration in murine liver carcinomas. Nature *445*, 656–660.

Yang, J. *et al.* (2007). AZD1152, a novel and selective aurora B kinase inhibitor, induces growth arrest, apoptosis, and sensitization for tubulin depolymerizing agent or topoisomerase II inhibitor in human acute leukemia cells in vitro and in vivo. Blood *110*, 2034–2040.

Young, A. R. J. *et al.* (2009). Autophagy mediates the mitotic senescence transition. Genes Dev. *23*, 798–803.

Yun, M. *et al.* (2009). p31comet Induces cellular senescence through p21 accumulation and Mad2 disruption. Mol. Cancer Res. *7*, 371–382.

Zhang, R. *et al.* (2005). Formation of MacroH2A-containing senescence-associated heterochromatin foci and senescence driven by ASF1a and HIRA. Dev. Cell *8*, 19–30.

Sadaie_Figure 1

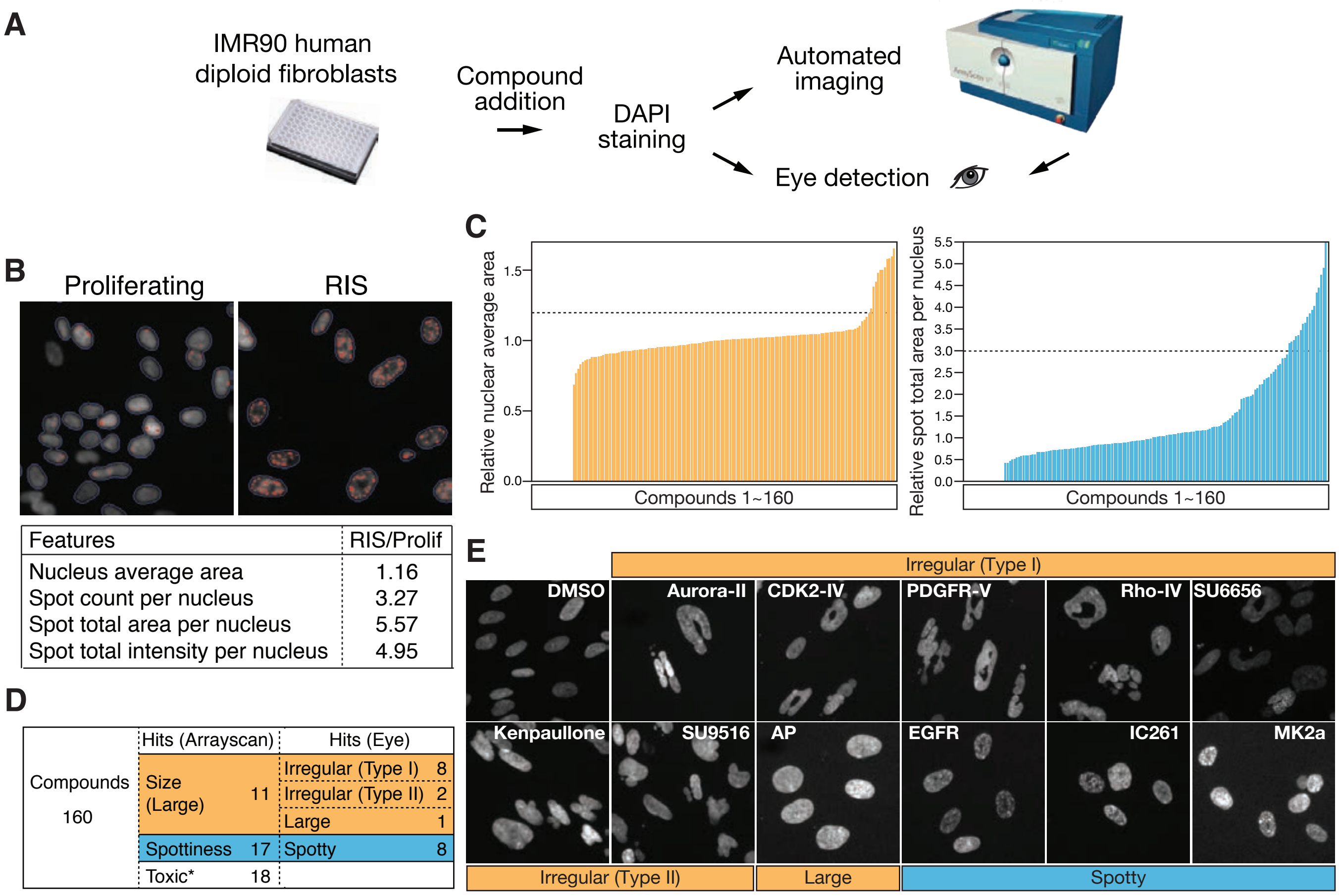

FIGURE 1. Automated image-based screening for compounds that induce morphological changes in nuclei. (A) Flow of the screen. Cells were treated with small molecule kinase inhibitors for 4 days in 96-well plates, followed by fixation and staining with DAPI, and analyzed using an automated image analyzer (Arrayscan), along with a visual inspection by fluorescent microscopy. (B) The protocol for automated nuclear image acquisition and analyses was set up using normally proliferating and H-RASG12V-induced senescent (RIS) IMR90 cells. Nuclei (DAPI signals) were recognized in the first channel (marked with blue contours), and then any spotty pattern was detected in the second channel (marked in red). Numbers represent the ratios between RIS and Proliferating (Prolif) cells for the indicated features. (C) Score distributions of the nuclear average area (left) or the spot total area per nucleus (right) of the cells after 4 days' exposure to 5 µM compounds. Threshold was set at 1.2-fold (relative nuclear average area) or 3-fold (relative spot total area per nucleus) of a DMSO control. (D) Number of the hits identified by the automated detection and subsequent eye detection. Cells were treated as in (C). *Toxic, compounds that failed to give more than 100 nuclei count. (E) Representative fluorescent images of nuclei of the cells treated with hit compounds by Arrayscan. Enlarged nuclei were categorized in three types, "Irregular type I", "Irregular type II", and "Large" according to their shape. Aurora-II, Aurora kinase inhibitor II; CDK2-IV, CDK2 inhibitor IV; PDGFR-V, PDGF RTK inhibitor; Rho-IV, Rho kinase inhibitor IV; AP, Aminopurvalanol A; EGFR, EGFR inhibitor; MK2a, MK2a inhibitor.

Sadaie_Figure 2

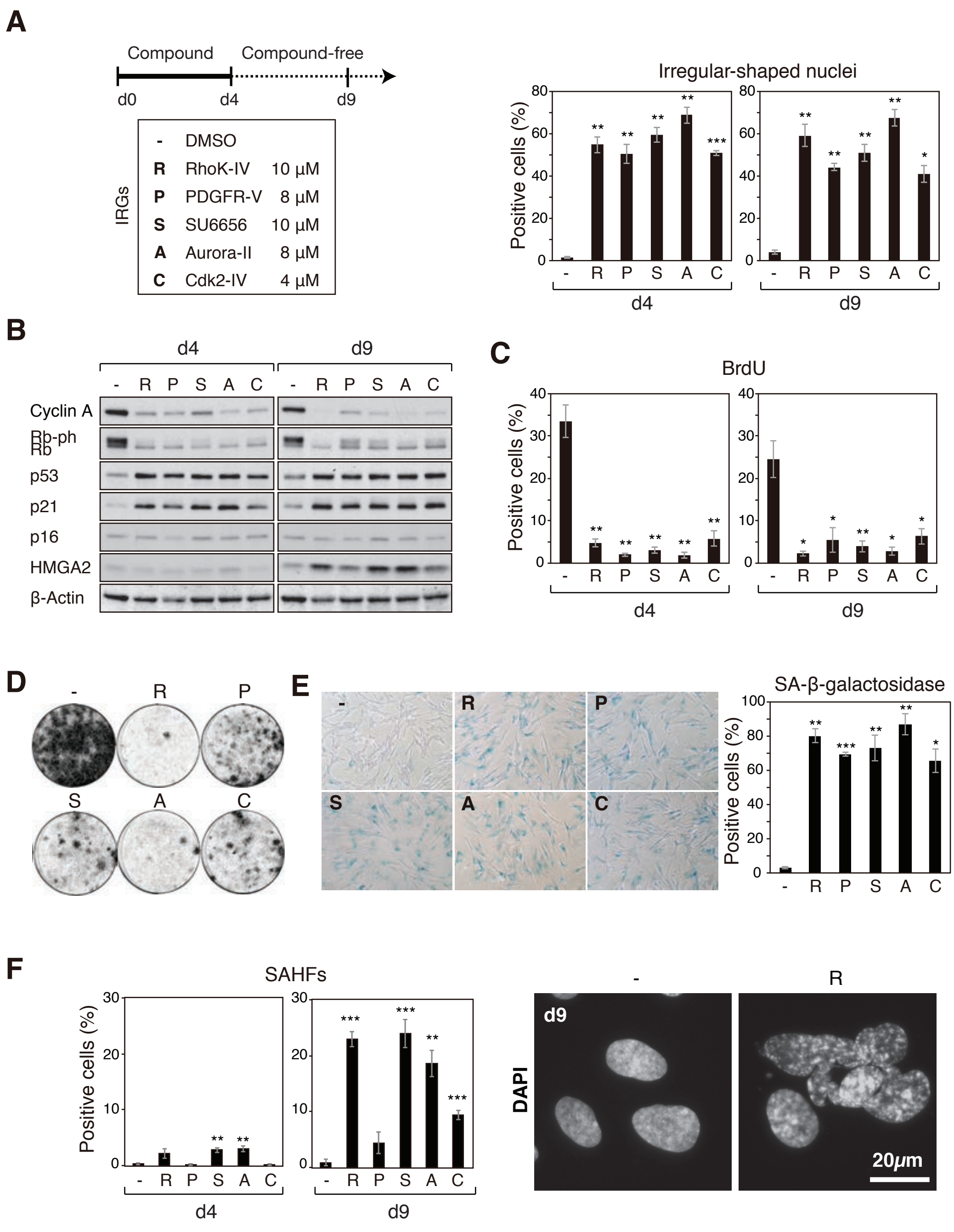

FIGURE 2. ‘Irregular-shaped’ nuclear phenotype is associated with cellular senescence. (A) IMR90 cells were exposed to the hit compounds that induce formation of the irregular-shaped nuclei (IRGs) for 4 days (d4), followed by a 5-day incubation in compound-free media (d9). The percentage of cells showing irregular-shaped nuclei at the indicated time points was assessed using DAPI staining. (B) Immunoblot analysis for the indicated proteins. RB-ph, phosphorylated RB. (C) Percentage of BrdU incorporation positive cells. (D) For colony formation assay, cells were plated without compounds after a 4-day treatment with IRGs. (E) SA-β-galactosidase activity in the compound-free cells (d9). (F) Cells indicated were assessed for SAHF formation. Values are mean ± SEM from 3 independent experiments. *$p < 0.05$, **$p < 0.01$, ***$p < 0.001$.

Sadaie_Figure 3

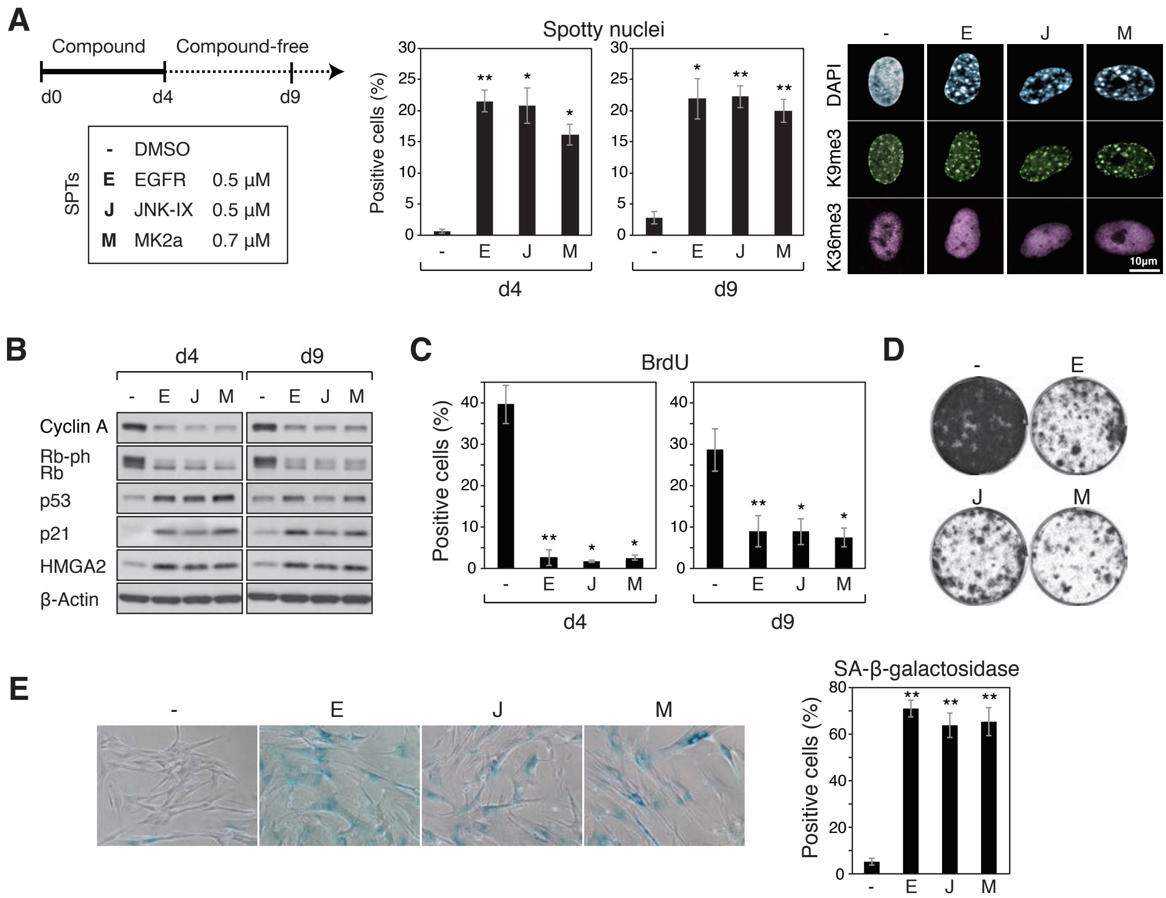

FIGURE 3. ‘Spotty’ nuclear phenotype is associated with cellular senescence.
(A) Cells were assessed for formation of a spotty nucleus using immunofluorescence. Right, confocal images of the cells immuno-stained for histone H3 tri-methylated at lysine 9 (H3K9me3) and H3K36me3, markers of heterochromatin and euchromatin, respectively, and counter-stained with DAPI. DAPI foci were colocalized with H3K9me3. (B) Immunoblot analysis in the compound-treated cells using the indicated antibodies. (C) Percentage of BrdU incorporation positive cells. (D) After a 4-day treatment with the IRGs, cells were plated without the compounds in equal number for the colony formation assays. (E) Senescence associated-β-galactosidase activities in the indicated cells at d9.

Sadaie_Figure 4

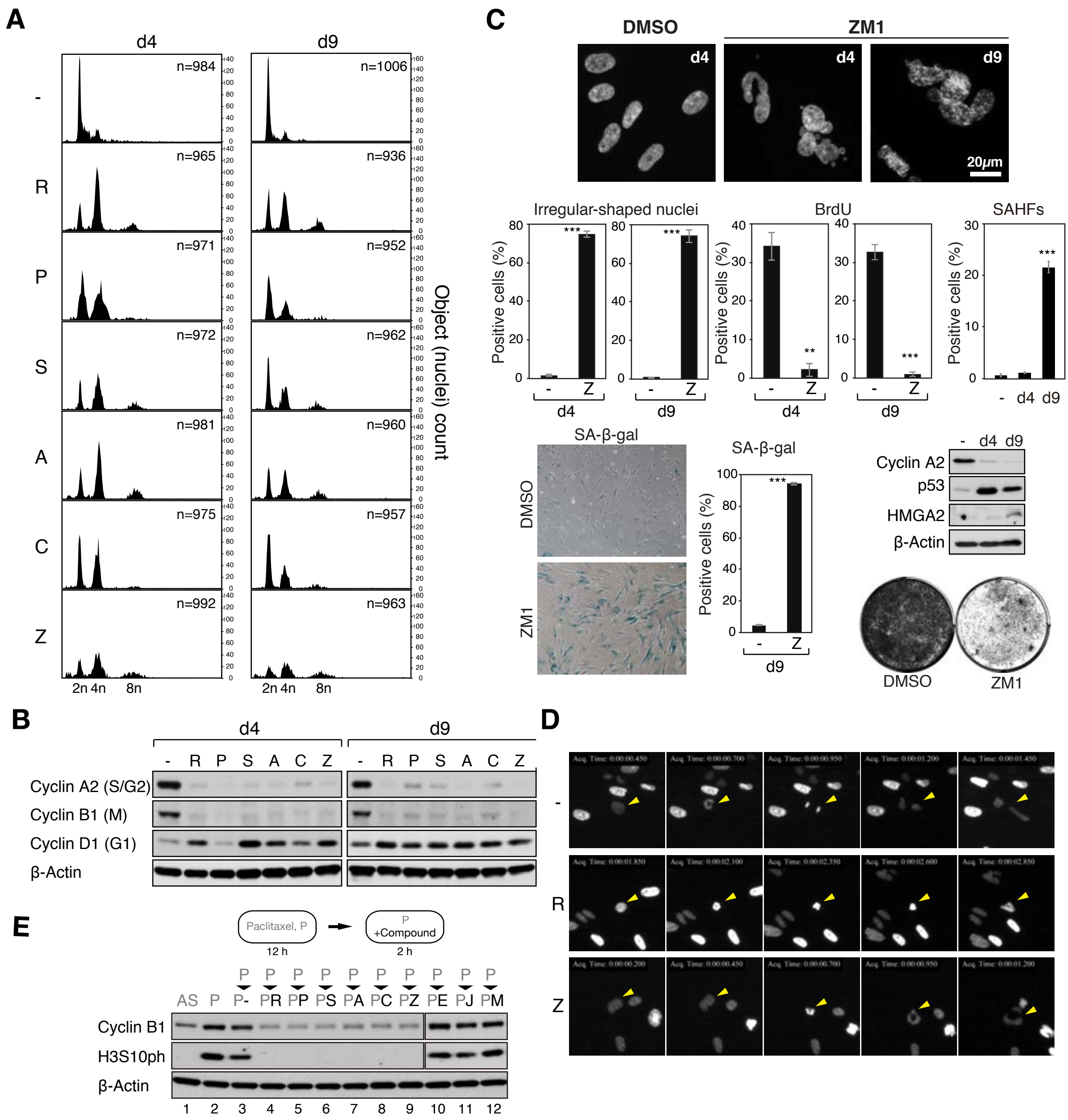

FIGURE 4. Aurora kinase inhibition phenocopies IRG-treatment in IMR90 cells (A) Cell cycle profiles of the cells treated as in Figure 2A were analyzed by laser scanning cytometry. In addition to IRG hits, an AURKB inhibitor ZM1 (2 μM) (Z) was included. (B) Accumulation of a G1 phase cyclin in the IRGs- or ZM1-treated cells. (C) ZM1-treatment induces senescence in IMR90 cells. Cells treated as in (A) were assessed for nuclear morphology, BrdU-incorporation, SAHF formation, SA-ß-gal activities, expression of indicated proteins, and colony formation. (D) Time-lapse images of the nuclei in compound-treated cells expressing H2B-EYFP (see Supplemental Movies S1-3). (E) Treatment of cells with IRGs elicits exit from paclitaxel-induced M phase arrest. IMR90 cells were synchronized in M phase by paclitaxel (P) for 12 hours, and thereafter the indicated hit compounds were added and incubated for 2 hours. For comparison, we also used the spotty hit compounds, which failed to induce a premature exit from the paclitaxel-induced M phase arrest (lanes 10-12, see Supplemental Figure S4). M phase cells were assessed using the levels of cyclin B1 and histone H3 phosphorylation at serine 10 (H3S10ph) (a direct substrate of AURKB). The blots for cyclin B1 and H3S10ph in the paclitaxel treated cells (left) were run in the same gel (see full lanes in Supplemental Figure S4).

Sadaie_Figure 5

A

Compound	IC50 (nM)		Nuclear phenotype
	AURKA	AURKB	
RhoK-IV	877	109	Irregular/Large
PDGFR-V	647	17	Irregular/Large
SU6656	1550	284	Irregular/Large
Aurora-II	943	110	Irregular/Large
CDK2-IV	87	48	Irregular/Large
ZM1	264	35	Irregular/Large
EGFR	>20000	>20000	Spotty
JNK-IX	>20000	>20000	Spotty
MK2	>20000	>20000	Spotty

B

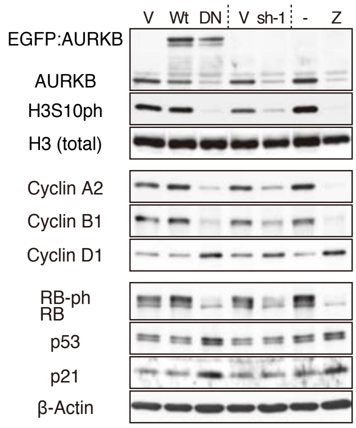

C

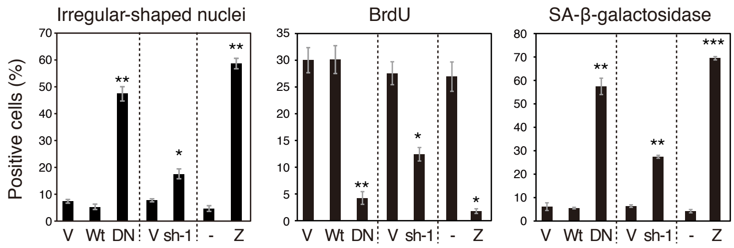

D

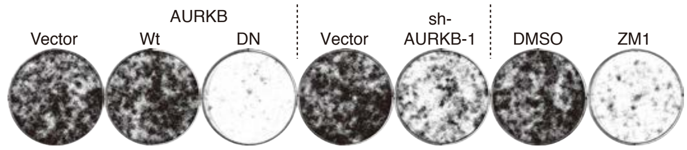

FIGURE 5. Specific inhibition of Aurora B kinase activity induces cellular senescence. (A) In vitro kinase activity assay. The IC50 of the indicated compounds was determined using an in vitro kinase activity assay for AURKA or AURKB. (B-D) Genetic inhibition of AURKB activity induces cellular senescence. IMR90 cells were stably transduced with retroviral vectors expressing EGFP-tagged wild-type (Wt) or kinase-dead dominant negative (DN) mutant (AURKBD218N) AURKB, sh-AURKB-1 (sh-1) (Supplemental Figure S6), or corresponding controls (V) (EGFP or miR30 vector, respectively). Cells were also treated with ZM1 (Z) or DMSO (-) for comparison (d9). At d6 after retroviral infection and selection, cells were assessed for protein expression (B), irregular-shaped nuclei, BrdU incorporation, and SA-β-galactosidase activity (C). Values are mean ± SEM from 3 independent experiments. *$p < 0.05$, **$p < 0.01$, ***$p < 0.001$. Cells were also plated at the same density and assessed for colony formation (D).

Sadaie_Figure 6

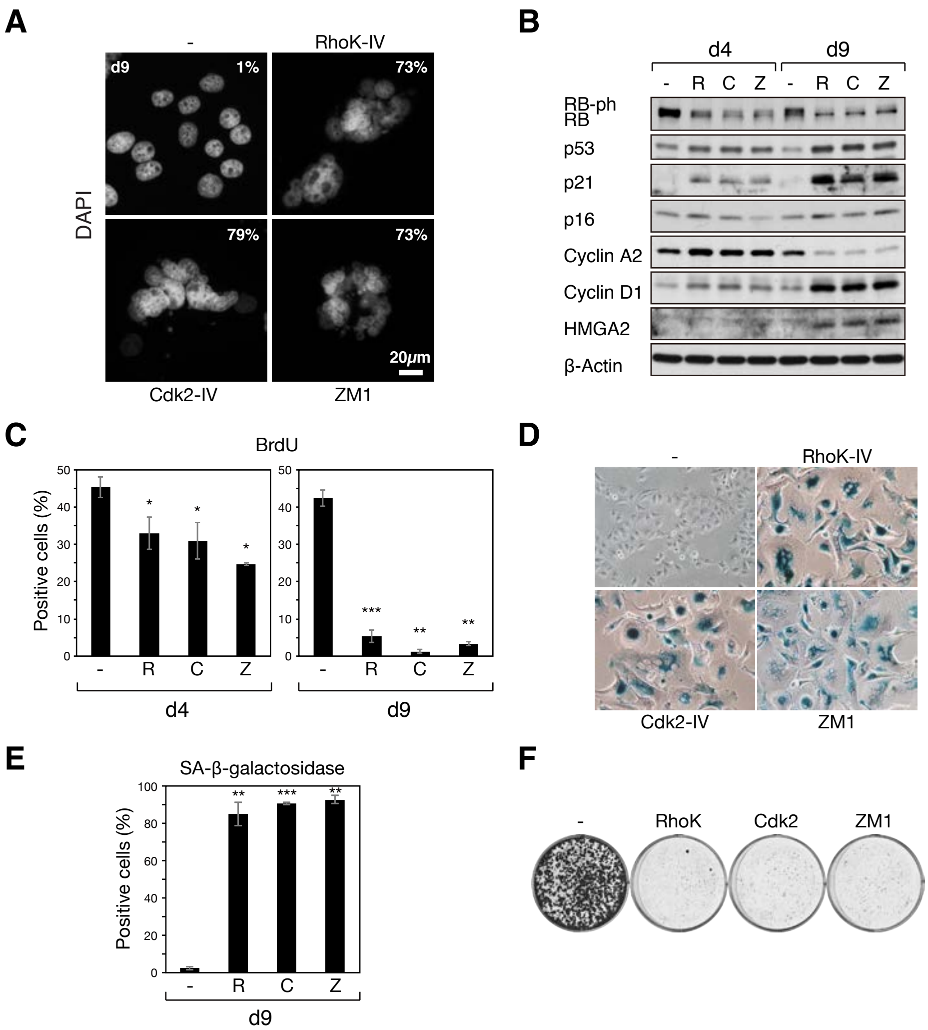

FIGURE 6. HeLa cells undergo cellular senescence by treatment with IRGs. (A) Fluorescent images of HeLa cells, which have been treated with selected IRG compounds and ZM1 for 4 days, followed by a 5-day culture in compound-free medium (d9) as in Figure 2A. The same concentrations except for ZM1, which was used at 1.5 μM, were used as in IMR90 cells (see Figure 2A). DNA was stained with DAPI. Numbers represent percentages of nuclei with an irregular shape (d9). (B) Immunoblot analysis for the indicated proteins in the HeLa cells at d4 and d9. (C) Percentage of cells that are BrdU incorporation positive. (D, E) SA-β-galactosidase assays for the compound-pre-treated HeLa cells at d9; representative images (D) and quantitative data (E). *$p < 0.05$, **$p < 0.01$, ***$p < 0.001$. (F) Colony formation assays in HeLa cells pre-treated with indicated compounds for 4 days. Values are mean ± SEM from 3 independent experiments.

Sadaie_Figure 7

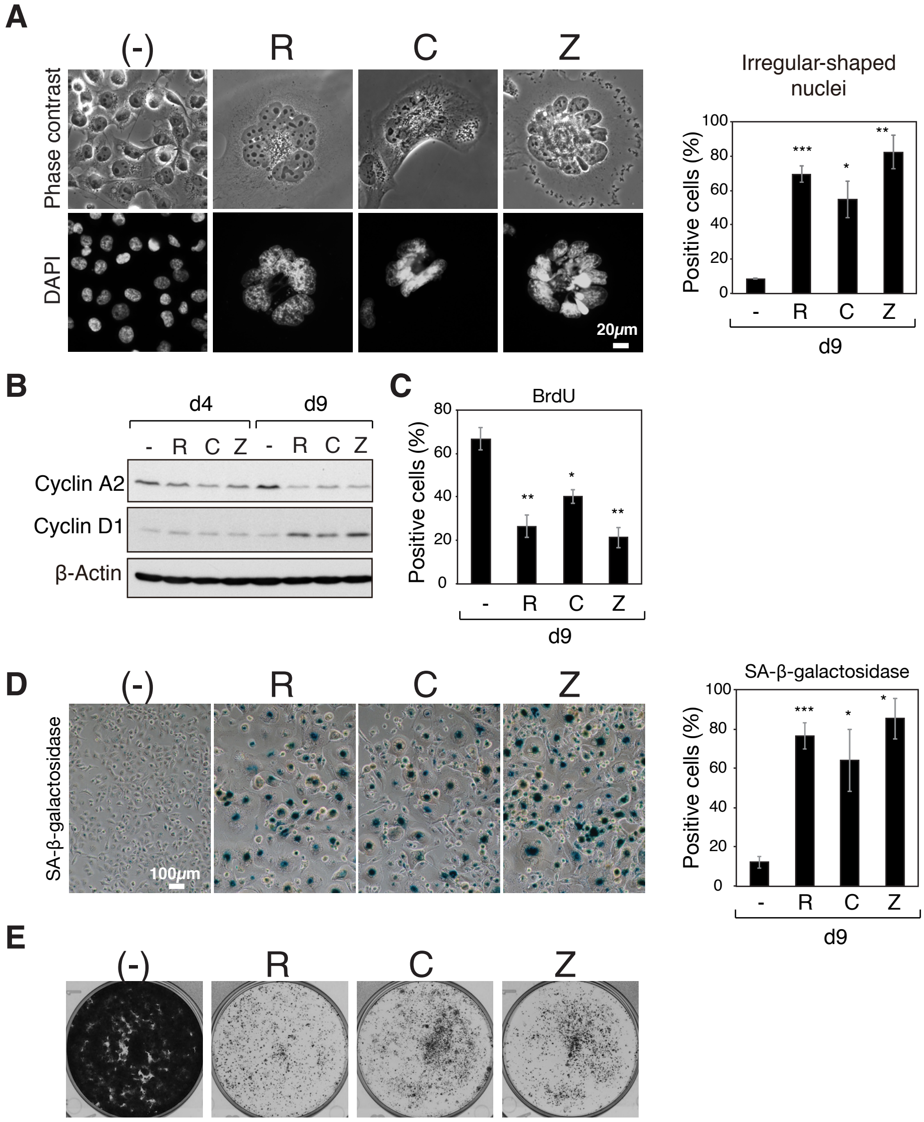

FIGURE 7. p53-null cancer cells undergo cellular senescence by treatment with IRGs. (A) Phase contrast and DAPI images of the H1299 cells, which were treated with selected IRG compounds and ZM1 for 4 days, followed by a 5-day culture in compound-free medium (d9) as in Figure 2A. (B) Immunoblot analysis for the indicated proteins in H1299 cells at d4 and d9. (C) Percentage of the BrdU incorporation positive cells. (D) SA-β-galactosidase assays for the compound-pre-treated H1299 cells at d9; representative images (D) and quantitative data (E). Values are mean ± SEM from 3 independent experiments. *$p < 0.05$, **$p < 0.01$, ***$p < 0.001$. (E) H1299 cells pre-treated with the indicated compounds for 4 days were maintained in normal media for colony formation assay.

SUPPLEMENTAL INFORMATION

Supplemental Figure Legends S1-8

Supplemental Movie Legends S1-3

Supplemental Figures S1-8

Supplemental Movies S1-3 (separate avi files)

Supplemental Tables S1-3

Sadaie_Figure S1

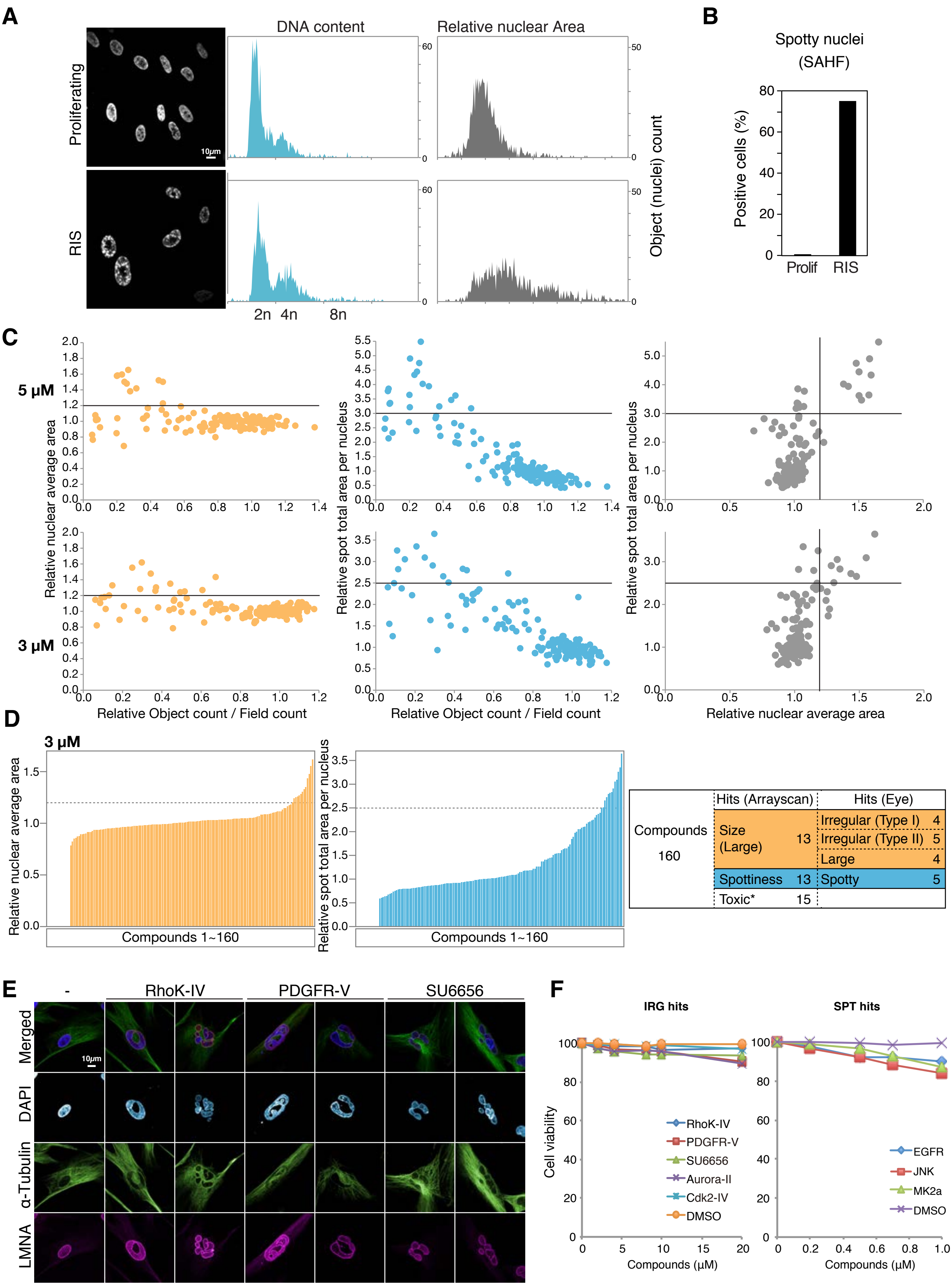

SUPPLEMENTAL FIGURE S1. Increased large and spotty nuclei in RAS-induced senescent cells. (A) Oncogenic RASG12V-induced senescent (RIS) IMR90 cells were stained with DAPI and assessed for DNA content and nuclear size using a laser scanning cytometer (iCys). (B) Percentage of SAHF-positive senescent cells was manually counted. Prolif, proliferating. (C) 2-D plots for the indicated parameters measured by automated detection using ArrayScan. Cells were treated with library compounds either at 5 µM (top) or 3 µM (bottom) for 4 days. An arbitrary threshold for relative nuclear average area (compounds/DMSO) (representing 'nuclear size') were set at 1.2 for both concentrations, whereas thresholds for relative spot total area per nucleus (compounds/DMSO) (representing 'spottiness') were set at 3 or 2.5 for 5 µM or 3 µM libraries, respectively. (D) Screening of compounds at 3 µM. Score distributions of relative nuclear average area or relative spot total area per nucleus were shown as in Figure 1C. Number of hits identified by automated detection and subsequent visual inspection are summarized (right). *Compounds that gave counts of less than 100 nuclei. (E) Confocal images of IMR90 cells treated with indicated compounds (d3). Cells were stained using the indicated antibodies. LMNA, Lamin A. (F) Cell viability was determined by trypan blue exclusion assay after 24h incubation of IMR90 cells with indicated compounds at different concentrations.

Sadaie_Figure S2

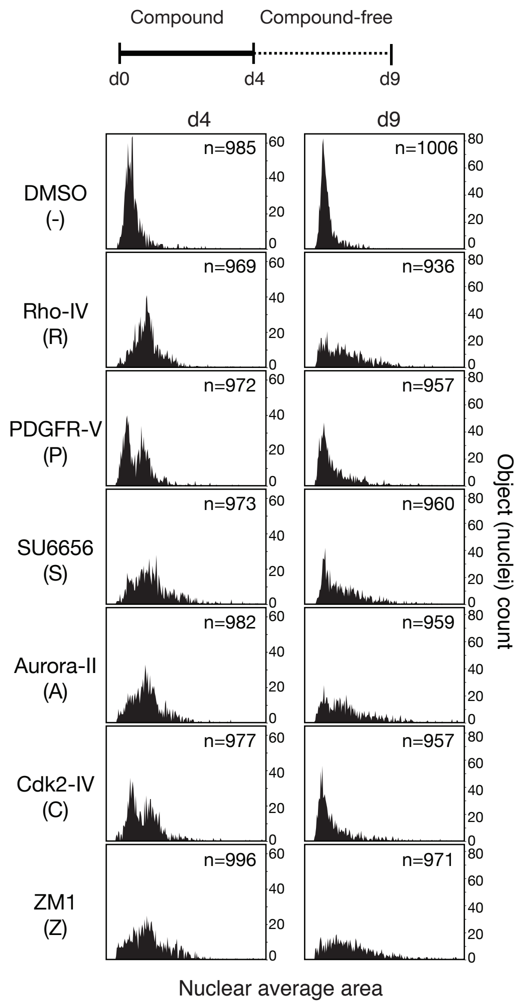

SUPPLEMENTAL FIGURE S2. Increased nuclear size in cells treated with the IRGs. Histograms show distribution of nuclear size in cells treated with the indicated kinase inhibitors as in Figure 2. Cells at d4 and d9 were stained with DAPI and analyzed by laser scanning cytometer.

Sadaie_Figure S3

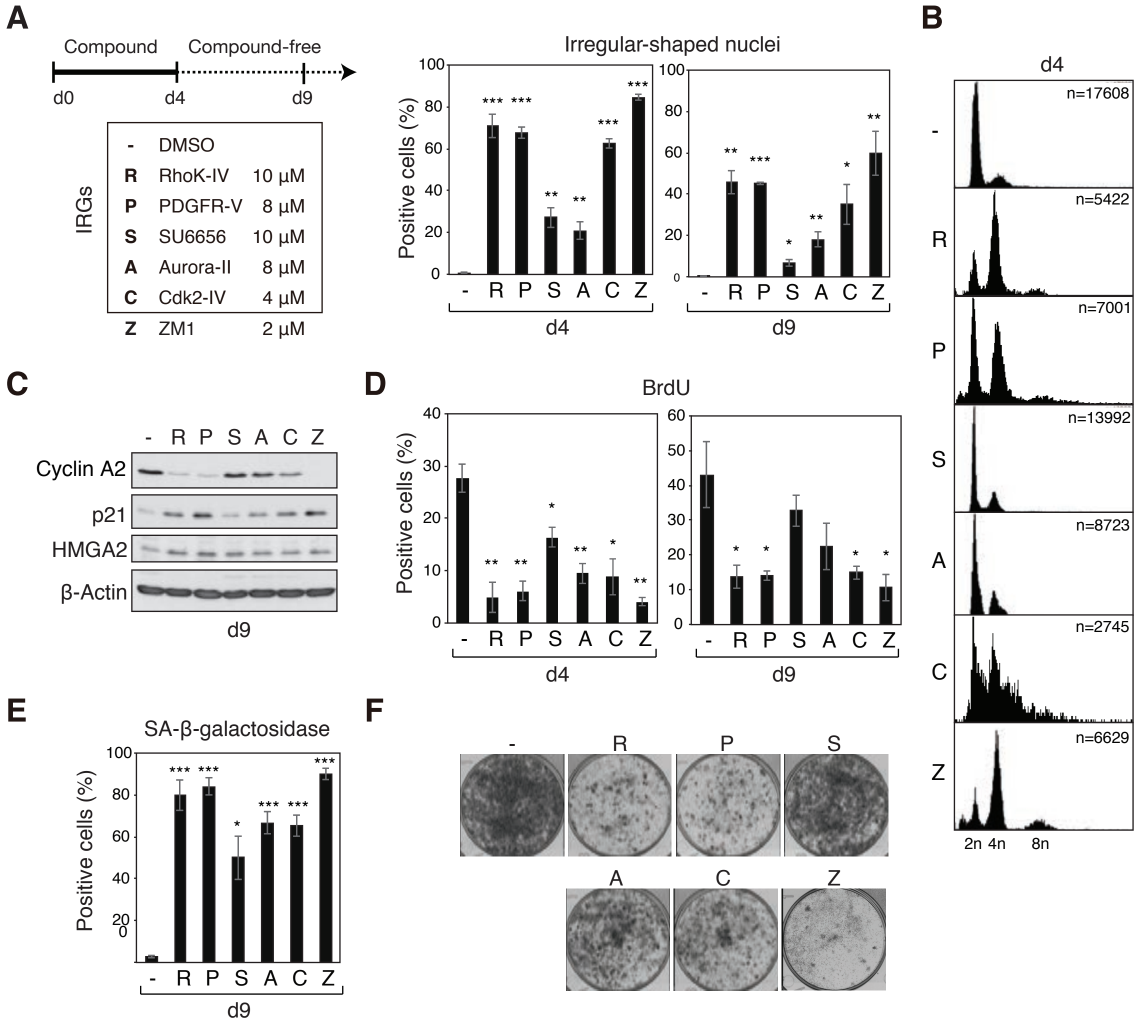

SUPPLEMENTAL FIGURE S3. Treatment with IRG hits or ZM1 induces senescence in BJ cells. (A-F) BJ cells were treated with indicated compounds as in Figure 2A, and assessed for nuclear shape (A), cell cycle profile (B), protein expression (C), BrdU incorporation (D), SA-β-galactosidase activity (E), and colony forming capacity (F). Values are mean ± SEM from 3 independent experiments. *$p < 0.05$, **$p < 0.01$, ***$p < 0.001$.

Sadaie_Figure S4

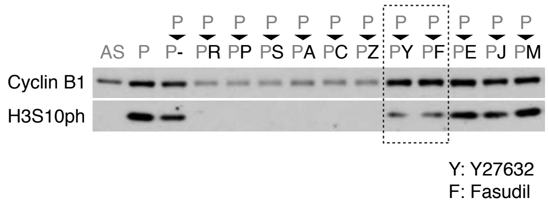

SUPPLEMENTAL FIGURE S4. Full lanes in blots shown in Figure 3E. Two lanes indicated were removed in Figure 4E, because these compounds are not directly related to the current study. Note as expected both compounds, which inhibit ROCK, also failed to elicit exit from paclitaxel-induced M phase arrest.

Sadaie_Figure S5

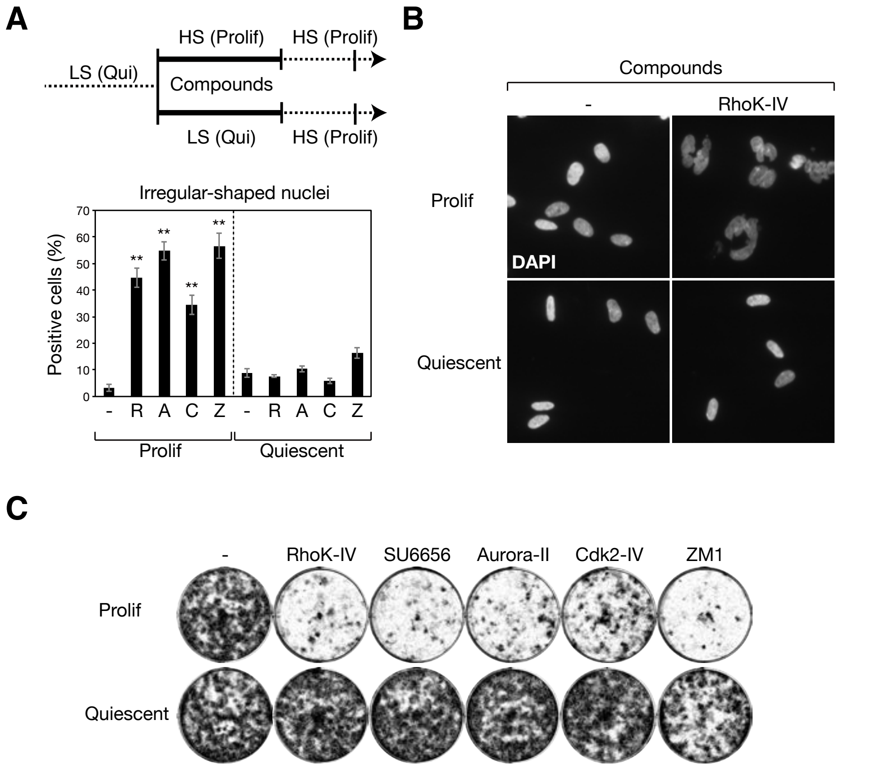

SUPPLEMENTAL FIGURE S5. Treatment of quiescent cells with IRGs or ZM1 does not have an impact on their proliferation after releasing from quiescence. (A, B) IMR90 cells were synchronized at quiescence (G0 arrest) by a 3-day incubation in low serum (0.1%) (LS) medium, and treated subsequently with IRGs/ZM1 either in high serum (10%) (HS) or LS medium for 3 days. After the treatment, compounds were removed and cells were incubated for 2 days in HS media and then assessed for nuclear shape. Percentages of cells that had irregular-shaped nuclei (A) and representative images of DAPI stained cells (B) are shown. Prolif, proliferating; Qui, quiescent. (C) Cells treated as shown in (A) with the indicated compounds were assessed for colony forming capacity. After removing compounds, all cells were maintained in normal medium (HS).

Sadaie_Figure S6

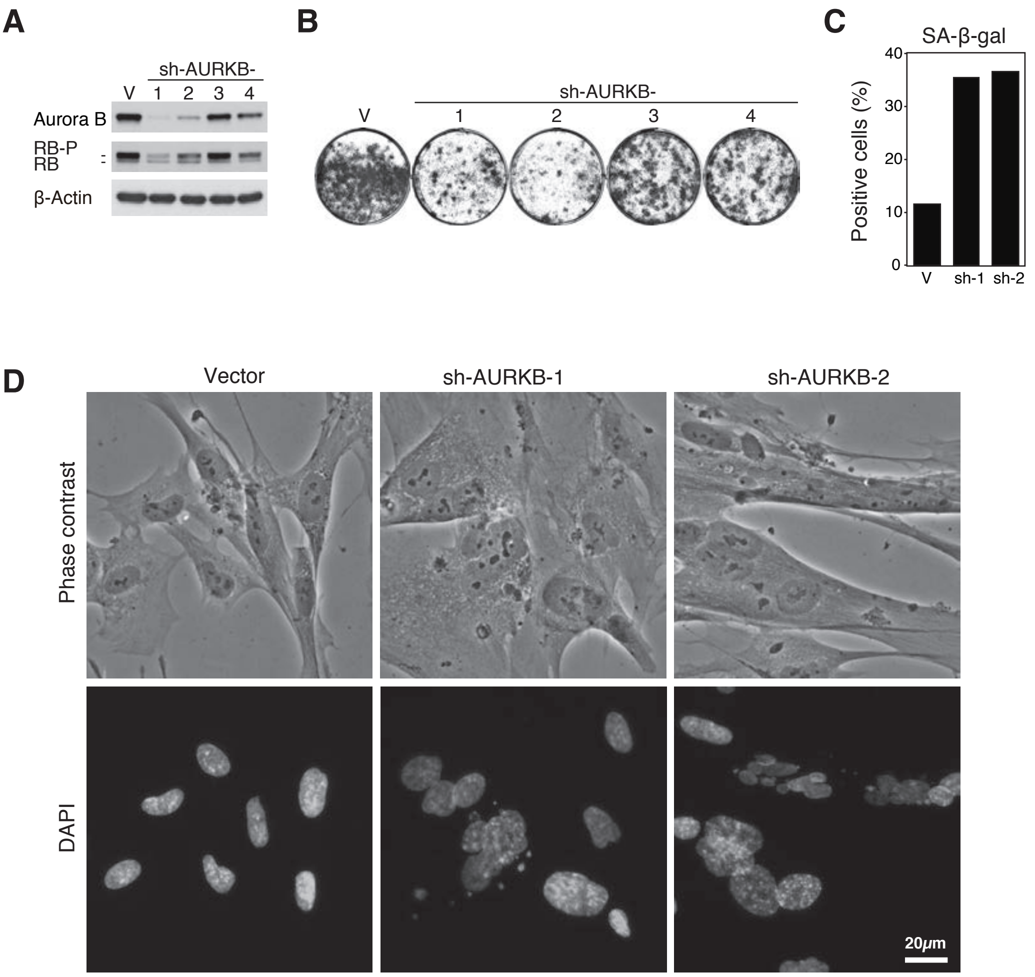

SUPPLEMENTAL FIGURE S6. Validation of AURKB shRNAs. (A) Western blotting for the indicated proteins in IMR90 cells stably expressing four different shRNAs against AURKB in a miR30 backbone. RB-P, phosphorylated RB. V, miR30-based RNAi vector. (B) Colony formation assay in indicated cells. (C) Percentage of SA-β-gal-positive cells in the indicated cells. Sh-1, sh-AURKB-1; sh-2, sh-AURKB-2. Data are representative from at least two independent experiments. (D) Phase contrast and DAPI images of the cells expressing sh-AURKB-1 or sh-AURKB-2.

Sadaie_Figure S7

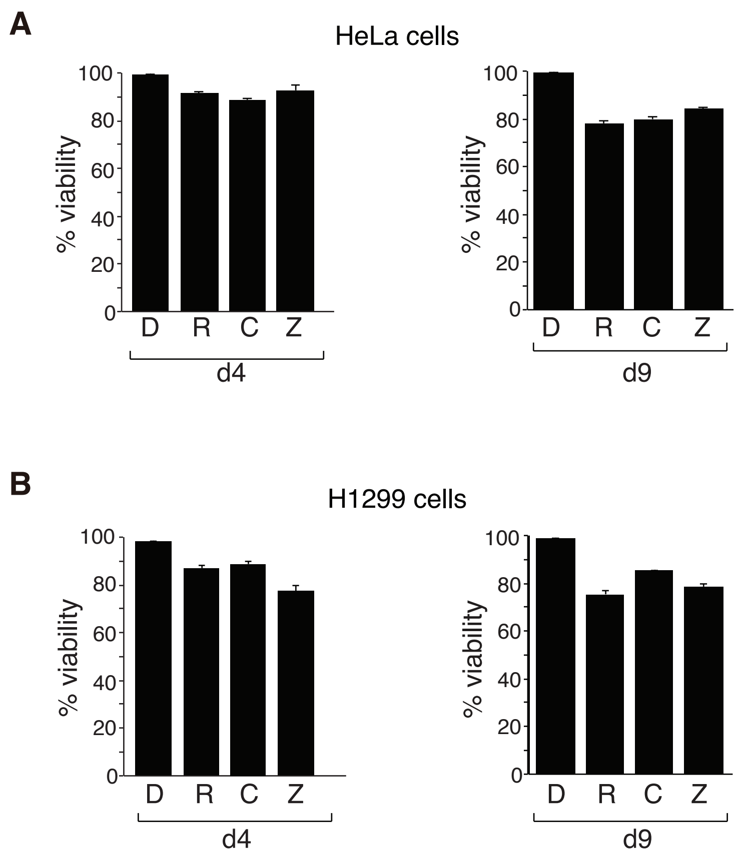

SUPPLEMENTAL FIGURE S7. Cell viability of tumour cell lines treated with IRG compounds. (A, B) HeLa cells (A) and H1299 cells (B) were treated with indicated compounds as in Figure 2A and cell viability was assessed by trypan blue exclusion. Cells were replated 24h before the assay.

Sadaie_Figure S8

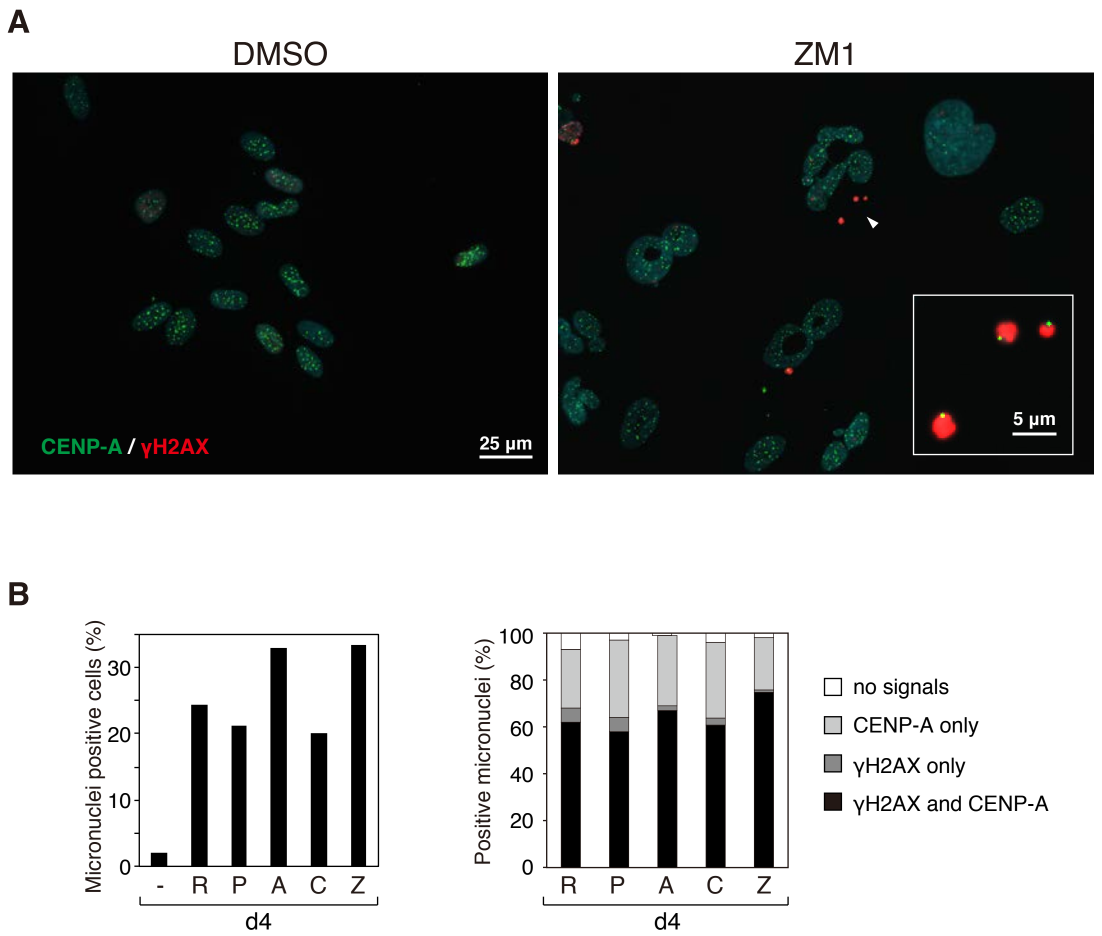

SUPPLEMENTAL FIGURE S8. Increased DNA damage and micronuclear formation in IRG-treated cells. (A) Representative images of cells treated with ZM1 or DMSO for 4 days. Green, CENP-A; red, γH2AX. (B) Percentage of cells with micronuclei (left) and proportion of micronuclei positive for γH2AX and/or CENP-A signals. Data are representative from at least two independent experiments.

SUPPLEMENTAL MOVIES S1-S3. IMR90 cells treated with compounds exit M phase without chromosome segregation. IMR90 cells expressing H2B-EYFP were synchronized at the G1/S border with double thymidine treatment, and released into medium containing DMSO or indicated compounds. Ten hours after the release, time-lapse images of H2B-EYFP were taken every 5 minutes. Movie S1. Representative time-lapse images of control cells treated with DMSO. Movie S2. Representative time-lapse images of cells treated with PDGFR-V (Large image field). Movie S3. Representative time-lapse images of cells treated with ZM1.

SUPPLEMENTAL TABLE S1. Optimized ArrayScan settings for detecting nuclear morphological changes.

Category	Parameter	Setting	Comments
Assay	Assay algorithm	SpotDetector.V3	Name of BioApplication – optimized for spot detection
	Protocol name	SAHF_compounds_20x_Spots	
	# channels	2 (both DAPI)	Allows collection of two images with differing saturation
	Form Factor	Falcon 96 well	Microplate template
Image Acquisition	Objective	20x	Highest magnification available to permit detection of distinct puncta
	Acquisition camera mode	Standard	Pixel resolution 1024x1024; 2x2 binning
	AutoFocus camera mode	AutoFocus	Pixel resolution 1024x1024; 4x4 binning (faster focusing)
Scan Limits	Max Fields for Well	60	Maximum number of images taken per well
	Min Objects for Well	600	Min # of objects (nuclei) to detectfor each well
	Max Sparse Fields for Well	4	# of images taken of 'Sparse wells' before moving to next well
	Min Objects for Field	5	'Sparse well' defined as one with <5 nuclei
Channel 1: Nuclei	Dye	XF100 - Hoechst	Name of fluorescence filter
	Exposure	Fixed: 40% saturation	These settings set the threshold for detecting nuclei as single objects (i.e. whole nuclei). Typical exposure time = 0.054secs. Threshold depends on signal intensity.
	Object identification	Fixed Threshold: 20 – 100	
	ObjectAreaCh1	Min: 200	Defines min and max size of a nucleus in pixels (eliminates debris and large nuclear clumps)
		Max: 2500	
	ObjectAvgIntenCh1	Min: 0	Rejects very bright objects – most likely debris
		Max: 2000	
Channel 2: Spots	Dye	XF100 - Hoechst	Name of fluorescence filter
	Exposure	Fixed: 25% saturation	Using a lower saturation helps improve sensitivity of spot detection. Typical exposure = 0.034secs
	Object identification	Fixed Threshold: 20 – 100	
	SpotAreaCh2	Min: 0	Defines min and max size of spots in pixels (improves assay sensitivity by eliminating larger areas of nucleus with different DAPI intensities)
		Max: 30	
Assay Parameters	Use reference wells	1	Turns on function which allows data to be expressed as % responders vs control wells. (Responder value set as 2SDs away from control)
	SpotDetectRadiusCh2	3	Determines the size of spots (in pixels) to be detected – helps to increase signal:noise by eliminating large variances in nuclear staining being detected as spots
	SpotSmoothFactorCh2	0	Turns off smoothing so that only bright spots with large contrast cf background are detected – improves signal:noise
	RejectBorderObjectsCh1	1	Rejects all nuclei at edge of image
	ObjectSegmentationCh1	0-7	Splits clumped nuclei into individual objects – important for assay sensitivity as SAHF phenotype is not 100% penetrant, and nuclear area is an important indicator of senescence
	Background CorrectionCh1	35	Improves signal:noise
	Background CorrectionCh2	10	

SUPPLEMENTAL TABLE S2. Size hits (nucleus average area)

Compound name*	Primary target kinases*	3 μM	5 μM
Aminopurvalanol A	Cdk1/cyclin B, Cdk2/cyclin A, Cdk2/cyclin E, Cdk5/p35	II	L
Aurora Kinase Inhibitor II	Aurora Kinase		I
Gö 6976	PKC	L	
Herbimycin A, Streptomyces sp.	P60$^{v\text{-}src}$	L	
JAK3 Inhibitor VI	JAK3		I
Met Kinase Inhibitor	met kinase activity		I
Rho Kinase Inhibitor IV	ROCK II	I	I
SU9516	Cdk2/A	II	II
BAY 11-7082	TNF-α-inducible phosphorylation of IκBα	L	Toxic
Cdk2 Inhibitor IV, NU6140	Cdk1/cyclin B	I	I
GSK-3 Inhibitor XIII	GSK-3	II	Toxic
IC261	CK1δ	L	
JAK Inhibitor I	murine JAK1	II	I
Kenpaullone	Gsk-3β	II	II
PDGF RTK Inhibitor	PDGFR	I	I
SU6656	Src	I	I
(Cut-off threshold)		(≥1.2)	(≥1.2)

Hits identified by Arrayscan are highlighted in grey
I: Irregular (Type I)
II: Irregular (Type II)
L: Large
Toxic: gives count of less than 100 nuclei per well
* as shown in the Merck Millipore website

SUPPELMENTAL TABLE S3. Spotty hits (spot total area per nucleus)

Compound name*	Primary target kinases*	3 μM	5 μM
Aminopurvalanol A	Cdk1/cyclin B, Cdk2/cyclin A, Cdk2/cyclin E, Cdk5/p35		-
Aurora Kinase Inhibitor II	Aurora Kinase		S
Chelerythrine Chloride	PKC	S	Toxic
Cdk2 Inhibitor III	Cdk2/A, Cdk2/E		S
EGFR Inhibitor	EGFR	S	S
GTP-14564	Class III receptor tyrosine kinases		S
Herbimycin A, Streptomyces sp.	$P60^{v\text{-}src}$	-	
JAK3 Inhibitor VI	JAK3	-	-
MK2a Inhibitor	Mk2α	S	S
Rho Kinase Inhibitor IV	ROCK II	S	S
SU9516	Cdk2/A	-	-
BAY 11-7082	TNF-α-inducible phosphorylation of IκBα	-	Toxic
Cdk2 Inhibitor IV, NU6140	Cdk1/cyclin B	-	-
EGFR/ErbB-2/ErbB-4 Inhibitor	EGFR/ErbB-2/ErbB-4		S
GSK-3 Inhibitor XIII	GSK-3	-	Toxic
IC261	CK1δ		S
JAK Inhibitor I	murine JAK1		-
JNK Inhibitor IX	JNK2, JNK3	S	
Kenpaullone	Gsk-3β		-
PDGF RTK Inhibitor	PDGFR	-	-
SB220025	P38MAPK		-
SU6656	Src	-	-
(Cut-off threshold)		(≥2.5)	(≥3.0)

Hits identified by Arrayscan are highlighted in grey
S: Spotty
-: Not obvious
Toxic: gives count of less than 100 nuclei per well
* as shown in the Merck Millipore website